International Journal of Automation and Computing
www.ijac.net

18(6), December 2021, 887-914
DOI: 10.1007/s11633-021-1313-0

Supervised and Semi-supervised Methods for Abdominal Organ Segmentation: A Review

Isaac Baffour Senkyire[1,2] Zhe Liu[1]

[1] School of Computer Science and Communication Engineering, Jiangsu University, Zhenjiang 212013, China

[2] Computer Science Department, Ghana Communication Technology University, Accra, Ghana

Abstract: Abdominal organ segmentation is the segregation of a single or multiple abdominal organ(s) into semantic image segments of pixels identified with homogeneous features such as color and texture, and intensity. The abdominal organ(s) condition is mostly connected with greater morbidity and mortality. Most patients often have asymptomatic abdominal conditions and symptoms, which are often recognized late; hence the abdomen has been the third most common cause of damage to the human body. That notwithstanding, there may be improved outcomes where the condition of an abdominal organ is detected earlier. Over the years, supervised and semi-supervised machine learning methods have been used to segment abdominal organ(s) in order to detect the organ(s) condition. The supervised methods perform well when the used training data represents the target data, but the methods require large manually annotated data and have adaptation problems. The semi-supervised methods are fast but record poor performance than the supervised if assumptions about the data fail to hold. Current state-of-the-art methods of supervised segmentation are largely based on deep learning techniques due to their good accuracy and success in real world applications. Though it requires a large amount of training data for automatic feature extraction, deep learning can hardly be used. As regards the semi-supervised methods of segmentation, self-training and graph-based techniques have attracted much research attention. Self-training can be used with any classifier but does not have a mechanism to rectify mistakes early. Graph-based techniques thrive on their convexity, scalability, and effectiveness in application but have an out-of-sample problem. In this review paper, a study has been carried out on supervised and semi-supervised methods of performing abdominal organ segmentation. An observation of the current approaches, connection and gaps are identified, and prospective future research opportunities are enumerated.

Keywords: Abdominal organ, supervised segmentation, semi-supervised segmentation, evaluation metrics, image segmentation, machine learning.

Citation: I. B. Senkyire, Z. Liu. Supervised and semi-supervised methods for abdominal organ segmentation: A review. *International Journal of Automation and Computing*, vol.18, no.6, pp.887–914, 2021. http://doi.org/10.1007/s11633-021-1313-0

1 Introduction

The abdomen is a vital and major part of the anatomical region of the human body between the thorax and the pelvis[1, 2]. The abdomen consists of major organs which are separated into four quadrants: left upper, right upper, left lower, and right lower quadrants. The left upper quadrant is anatomically associated with the spleen, stomach, body of pancreas, splenic flexure, and left suprarenal gland. The right upper quadrant is associated with the liver and gallbladder, duodenum, pylorus, hepatic flexure, and the right suprarenal gland. The left lower quadrants consist of the sigmoid colon, the ovary and uterine tube, left ureter, and descending colon. The right lower quadrant has the cecum and appendix, ovary and uterine tube, right ureter and the ascending colon. The quadrants assist in distinguishing the abdominal organ′s location for the examiner[3]. The abdominal organs play critical individual roles and also supports other functions of the entire human body[4], that notwithstanding the abdomen is noted to be the third most common cause of damage of the body organ. A greater percentage of patients often have asymptomatic abdominal condition and symptoms[5], and late recognition of the abdominal organ′s condition is mostly linked with greater amount of morbidity and mortality[6, 7]. However, there is improvement in outcome when abdominal organ condition is detected earlier[8]. Accessing or examining these organs of the abdomen has been a paradox although its anterior technique is soft and flexible when it is calm, and the organs are not microscopic. While there are some possible exceptions generally, the abdominal internal organs normally are not detectable on physical examination, rather medical imaging methods are used[1].

Medical imaging is a technique used to view the internal parts of the human body by creating visual representations of some organs or tissues[9], otherwise known as bio-medical images, and further applying the techniques

Review
Manuscript received April 7, 2021; accepted October 12, 2021
Recommended by Associate Editor Shan Yu
Colored figures are available in the online version at https://link.springer.com/journal/11633

of image processing for the purposes of diagnosis and therapy. Different imaging technology such as light (endoscopy, optical coherence tomography (OCT)), radioactive pharmaceuticals (nuclear medicine: position emission tomography (PET), single photon emission computed tomography (SPECT)), magnet (magnetic resonance imaging (MRI)), sound (ultrasound (US)), or X-rays (computed tomography (CT) scan) can be used to capture the bio-medical images for medical image analysis which will facilitate highly accurate diagnosis by assessing the current condition[10], structure and functions of the abdominal organ or tissue, abdominal organ disease monitoring[11], further analysis[9] and diagnosis[12].

In order to obtain effective bio-medical images, techniques to process the medical image play an important role in medical imaging. Firstly, the image needs to be acquired, followed by the varied image processing techniques: image enhancement, image segmentation, feature extraction and selection, and image classification. Of all the image processing techniques, image segmentation is the most significant stage in the analysis of medical images. It facilitates the extraction and visualization of the region of interest (ROI) for additional analysis[9], image-guided interventions, enhanced radiological diagnosis, radiotherapy[13], etc. Image segmentation is the division of every single component present in an image into a set of groups with common property[10]. This is technically explained as the process in which each pixel in an image is assigned a label, and there is a connection of the pixels with the same label with respect to some semantic or visual property[14]. Of particular interest, the segmentation of the organ(s) of the abdomen creates a view of the abdomen of the body[9], where a single abdominal organ[15–18] or multiple abdominal organs[19–21] is or are segregated into semantic image segments[22] of pixels identified with homogeneous features such as color and texture[9], and intensity[23] for computer-aided surgery (CAS), radiation therapy planning[20], anatomical structure modeling, measurement of tumor growth[24] and visualization prior to diagnosis, treatment, and surgical procedures, and computer-aided diagnosis[19] which can save the life of patients[12].

The techniques for machine learning based segmentation methods are grouped into two main categories: supervised and unsupervised segmentation methods[25–27]. Both supervised and unsupervised abdominal segmentation methods have been highly effective at producing accurate results. For example, the supervised methods produce accurate results with a large training dataset and ground truth. The unsupervised methods on the contrary produce accurate results without manually labeled dataset[28]. However, it is extremely costly to create a large library of annotated images to represent the manifold of possible abdominal images. Yet, there is an abundance of unannotated data, which is typically cheaper compared to the annotated data. This has attracted the attention of the research community to combine the limited labeled data and the abundant unlabeled data in a learning approach known as semi-supervised method[29].

To the best of our knowledge, there have been several review works that have focused on the varied methodologies and technical approaches used on individual abdominal organ′s segmentation[30–32] using some contemporary medical imaging modalities and its progress based on automated segmentation mechanism[33–35] and [36] which focused on deep learning for single and multi-abdominal organ(s) image segmentation, detection, classification and other related tasks. However, none of them have provided a systematic overview focused on abdominal organ(s) segmentation based on supervised and semi-supervised methods.

Web of Science core collection, Scopus and PubMed databases were initially queried for papers containing (“Abdominal organ segmentation” or “abdomen organ segmentation” or “multi-organ segmentation” or “supervised segmentation method” or “abdominal organ supervised method” or “abdominal organ supervised segmentation learning” or “semi-supervised segmentation method” or “abdomen organ semi-supervised method” or “abdomen organ semi-supervised segmentation learning”) in title or abstract. Also, Medical Image Computing and Computer Assisted Intervention Society (MICCAI), International Symposium on Biomedical Imaging (ISBI) and European Medicine and Biology Conference (EMBC) proceedings were searched based on the paper title. Papers that did not focus primarily on segmentation issues, and those not published in English were not considered.

This review aims to provide an overview of the supervised and semi-supervised methods of performing abdominal organ segmentation. It describes the connection and identifies the gaps in the current approaches, and enumerates prospective opportunities for future research. The review is targeted at medical image analysis researchers and any other interested parties.

The rest of this paper is organized as follows. Section 2 reviews methods of supervised and semi-supervised segmentation. Section 3 presents supervised abdominal segmentation methods and their application on single and multi-organs. Section 4 highlights semi-supervised abdominal segmentation methods relative to single and multi-organs. Section 5 does an assessment of datasets in line with abdominal organ segmentation. Section 6 presents a discussion and projection of future works.

2 Methods

2.1 Supervised segmentation methods

The supervised segmentation method uses prior knowledge, based on manual annotations[37] or labeled

images[27] to locate objects of interest in an image[38], and to assess how reliable the segmentation results are. The supervised method uses real objects[39]. The supervised segmentation method, regardless, has two downsides; it requires large manual annotated data[40, 27], and it has domain adaptation problem[37]. The method′s data for training is a pair which consists of input and output objects. The training data pairs have a function that learns from it to predict new samples[41]. The method notwithstanding performs well when the used training data is representative of the targeted data. Also, the supervised segmentation methods have broader applications and are more precise when provided with enough user input[42].

The supervised abdominal segmentation method adapts a semi-automatic segmentation[43, 44] process, and interactive segmentation, which produces objects prior[37] to guide a computer-aided abdominal organ segmentation through user interactions. The user input can be for instance, setting the contour to commence the segmentation or initializing a pixel or voxel seed point[45]. In supervised learning, a training set $D_S = \{(x_i, y_i)\}$, where every sample $x_i \in X$ is related to a label $y_i \in Y$. X is the feature space, like an m-dimensional space of real numbers $\mathbf{R}^m$, and Y is the label space, like the set {0, 1} for a binary classification problem or the set $\mathbf{R}$ for a regression problem. The data is used to train a classifier $f : x \to y$ that can make available labels for samples that are unlabeled from a previously unseen test set D_T[46].

Supervised segmentation methods are classified into Atlas-based segmentation methods[25], conventional supervised methods[47], and deep learning methods[48, 49]. In the 1990s, research studies of abdominal organ segmentation focused on atlas-based methods. The atlas-based methods use labeled images (i.e., atlas) entire content, making them more flexible regarding expected anatomical variations between subjects[50]. However, they were problematic, since they could not capture abdominal regions large inter-subject variations, and the time for computation was dependent tightly on the number of atlases[51]. Nonetheless, the past decade has registered a rigorous study of conventional supervised segmentation techniques such as support vector machine (SVM), random forest (RF), and k-nearest neighbor clustering. Though such techniques have been explored, they are limited in delineating fuzzy boundaries of abdominal organs in radiological images. Recently, there has been a significant progress in attaining segmentation results that are more accurate within the supervised framework of machine learning. This has been due to the significant shift from the manual to automatic feature extraction enabled by deep learning networks joined with the substantial improvement in computational power[25]. Supervised deep learning methods notwithstanding require a large amount of training data to extract features automatically[52, 25], otherwise, the methods can hardly be used[49].

2.2 Semi-supervised segmentation (SSS) methods

The semi-supervised segmentation method combines supervised model training and unsupervised feature representation learning[53], but it is a variance of the weakly supervised method[54, 55]. Semi-supervised learning involves a dataset X which consists of a small number of labeled samples and a large number of unlabeled samples, i.e., $X = \{X_l, X_u\}$, where $X_l = \{(x_i, y_i)\}_{i=1}^{l}$ depicts the labeled portion and $X_u = \{x_i\}_{i=1}^{u}$ depicts the unlabeled samples. Assume that the total number of samples for training is $N = l+u$ and practically $l \ll u$. The SSL goal is to learn the function predicted for the labels of those unlabeled samples by exploiting the information of the label dependency reflected by the information of the available label[56]. A semi-supervised method can be either transductive SSL or inductive SSL, otherwise known as the pure semi-supervised method. The inductive SSL is used to predict labels for future data, while the transductive SSL is used for predicting labels for the already available samples that are unlabeled[46, 54]. The semi-supervised segmentation method attempts to automatically exploits larger unlabeled data and less manually annotated or labeled data to improve learning performance, where no human interaction is assumed[48, 54]. It is identified as one of the approaches that tackle small training dataset and it leverages segmentation collections to generate anatomical priors[57].

The semi-supervised abdominal segmentation method utilizes data that is unlabeled to update or re-arrange labeled data hypothesis obtained. The method learns from both labeled and unlabeled abdominal organ images and it is fast. Generative method, self-training and co-training, graph-based method, and transductive support vector machine (TSVM) are the main categories of semi-supervised methods[26, 51].

Semi-supervised approaches, typically work by making further assumptions that connect properties of the input features distribution to properties of the decision function. The assumptions include: the smoothness assumption, i.e., in feature space, samples that are close together are likely to be from the same class; the cluster assumption, i.e., samples in a cluster are assumed to be from the same class; and the low density assumption, i.e., class boundaries are assumed to be in a feature space area that has a density lower than the clusters[46].

The generative semi-supervised method utilizes a parametric model which has both labeled and unlabeled abdominal organ data coming from the same inherent model[54], $q(u, v) = q(v)\ q(u|v)$, where $q(u, v)$ identifies a mixture distribution with a greater number of unlabeled abdominal organ data. Also, the components of the mixture can be known and those components associated with each of the classes are used to classify the unlabeled abdominal organ data samples. This model is noted to be

one of the oldest semi-supervised learning method, and it is very simple with a probabilistic structure, but it is difficult accessing its accuracy[26].

The self-training semi-supervised model propagates labels from the labeled to the unlabeled data, and then leverages on the larger, newly labeled set for training[46]. Self-training is an algorithm that is incremental in nature. The model works by first training a single classifier with a small amount of labeled abdominal organ data. This is followed by iteratively using the classifier to predict the unlabeled abdominal organ′s data′s labels, and the procedure recurs till there is some satisfaction of convergence criteria[51]. Finally, the labels of the unlabeled data ranked as most definite unlabeled points together with their outcome are put together into the training set of the labeled abdominal organ data[26]. The model makes and exploits the cluster assumption which presupposes that the method′s predictions are correct[46]. The self-training SSL model uses its own prediction to teach itself and it requires only a few labeled samples. However, the algorithm′s performance is dependent on the prediction confidence estimates[26], and it also does not have the mechanism to rectify mistakes early, hence, it hurts performance[58].

Co-training semi-supervised model, unlike the self-training model has more than one classifier trained and it yields more precise and robust outcomes. This model divides features into two independent sets, where each set is enough to train a good classifier with the labeled abdominal organ data. The learning process involves every classifier being re-trained with the other classifier′s training examples[26, 51]. Zhou et al.[51] identify multi-view learning as one of the commonly used models for semi-supervised learning, which outlines paradigms in learning by making use of the agreement that exists amongst varied learners, while they site co-training as one of the earliest multi-view learning schemes. Co-training SSL can evaluate features simultaneously but fails in a strongly correlated base learner′s predictions[26].

Graph-based SSL is an efficient method with computational simplicity and a better generalization ability[26] that generates a graph, where the nodes are made up of the training samples. Its edges depict some instances of similarity or distance relation. The method uses some criteria to propagate the information of a label on the graph, and its performance is dependent on the construction of the graph. The graph-based semi-supervised method is typically transductive and has scalability issues; a graph generated would need to be reconstructed if new instances should be accommodated[54]. Furthermore, the model assumes that samples connected are likely to have the same label. For instance, every pixel can be depicted as a node, and pixels that are of close proximity in the image, can be linked by edges. This seeks to propagate the labels along the graph. This can be realized using a graph cut algorithm, which locates the labeling of the pixels so that all the pixels produced are smooth along the graph. Nevertheless, locating a labeling means that images that were previously unseen cannot be labeled without running the procedure once more, also known as the out-of-sample problem[46].

TSVM is a semi-supervised model that uses unlabeled data to expand standard SVMs. With TSVM, the training set is divided into two independent sub-sets: labeled and unlabeled data. The TSVM exploits the data that is in abundance in order to update the decision boundary that has been constructed initially from a small number of labeled data while exploring the regions of low density. It attempts to classify the labeled examples correctly. TSVM model is effective with few labeled samples and has less computational cost than self-training and co-training[26]. However, TSVM is severely impeded in large-scale due to the high computational cost and non-convexity though it is a powerful semi-supervised learning model[59]. The model also focuses only on a specific working set. Hence, it has a generalization problem and performs poorly with new data[60].

Cheplygina et al.[46] cite the semi-supervised method to perform worse than the supervised if the additional assumptions about the data fail to hold. Cheplygina et al.[46] stipulates that recent approaches do not make additional assumptions about the data, instead they use assumptions which are already present in the classifier.

In this section, we first reviewed supervised segmentation methods, which were classified into atlas-based, conventional, and deep learning methods. From the literature reviewed, research works on the liver, kidney, gallbladder, pancreas, spleen, and multi-organ(s) using supervised segmentation methods have attracted increasing interest with deep learning, which indicates a shift from the atlas and conventional methods of segmentation. We also reviewed generative, self-training and co-training, graph-based, and transductive support vector machine methods which are the categories of the semi-supervised methods and their applications to the liver, kidney, gallbladder, pancreas, spleen, and multi-abdominal organs segmentation. From the literature reviewed, research works on the liver, kidney, gallbladder, pancreas, spleen, and multi-organ(s) using semi-supervised segmentation methods have attracted increasing interest with self-training, and graph-based methods.

3 Applications based on supervised segmentation method

This section provides a summary of supervised abdominal segmentation applications for single abdominal organs and multi-abdominal organs.

3.1 Single abdominal organ segmentation

In this section, we present an overview of the follow-

ing single abdominal organs: liver, kidney, gallbladder, pancreas, and spleen. The organs are introduced, their mortality rates and various diseases that affect the organs are also highlighted, and some research works based on supervised segmentation methods are outlined. Table 1 gives an overview of the supervised segmentation method applications as regards the specified organs.

3.1.1 Liver

The liver is the largest abdominal organ in the human body, which performs critical life sustaining tasks such as storing of vitamins and detoxification[116]. It is mostly threatened by diseases and drug damage[117]. Approximately 2 million deaths are recorded worldwide as a result of liver disease, half of the number is due to complications of cirrhosis, and the other half is also due to viral hepatitis and hepatocellular carcinoma (HCC). Cirrhosis currently accounts for 1.16 million deaths globally, and liver cancer with 788 000 deaths, making them the 11th and 16th ranked causes of death, respectively, each year, which is 3.5% of all deaths worldwide. Liver diseases can be categorized into alcohol-associated liver disease (AALD), non-alcoholic fatty liver disease (NAFLD), viral hepatitis (Hepatitis A, B, C, D, and E), primary sclerosing cholangitis, primary biliary cholangitis, autoimmune hepatitis, Wilson′s disease, and drug-induced liver injury. These diseases result in acute liver failure, compensated and decompensated cirrhosis, acute-on-chronic liver failure, and HCC[118]. Accordingly, liver segmentation is of prime importance in the diagnosis of liver diseases, functional assessment and treatment[119]. Over the years, research work has been done beyond the traditional manual approach to segment the liver: vessel tree[64],

Table 1 Overview of supervised method applications. The last column describes the type of supervised method.

Reference	Abdominal organ	Application	Supervised method
[61]	Liver	Tracking tumor position in ultrasound (US) images	Bi-directional convolutional long short-term memory network (LSTM) U-Net with densely connected convolutions bi-directional convolutional LSTM U-Net with densely connected convolutions (BCDU-Net) and convolutional neural network (CNN)
[62]		HCC liver tumor segmentation	Random forest (RF)
[63]		CT images liver segmentation	Contour embedded neural network (CENet)
[64]		Liver vessel segmentation	Deep neural network (DNN)
[65]		Segmentation and classification of liver tumor from CT images	Support vector machine (SVM)
[66]		Automatic segmentation of livers and liver tumors in CT images	Modified U-Net (mU-Net)
[67]		Liver segmentation for fusion-guided intervention	Multi-scale input and multi-scale output feature abstraction network (MIMO-FAN)
[68]		Automatic CT imaging liver segmentation in selective internal radiation therapy (SIRT)	DeepMedic (Modified CNN)
[69]		Liver segmentation and volumetry	Gaussian mixture model method and U-Net
[70]		Liver CT segmentation and classification	SegNet
[71]		Liver segmentation and classification of hepatobiliary phase (HBP) images for ethoxybenzyl diethylenetriamine pentaacetic acid-enhanced magnetic reasoning imaging (EOB-MRI) examination	CNN with U-Net architecture and HBP-CNN classification network
[72]		Liver and lesion segmentation	Cascaded U-Net (CU-Net)
[73]		Hepatic lesion segmentation	Modality weighted U-Net (MW-UNet)
[74]		Liver segmentation	Multiple atlas approach (Expected label value ELP computation approach)
[75]		MRI liver segmentation	Dilated FCN and modified U-Net
[76]		Automatic liver segmentation	SVM and neural network (NN) classifier
[77]		Liver segmentation in perfusion MR images	Probabilistic atlases
[78]		Liver segmentation	Faster R-CNN and DeepLab
[79]		Automated segmentation of volumetric medical images	Deep CNN (3D deeply supervised network and conditional random field model 3D-DSN+CRF)
[80]		Liver segmentation and lesions detection	Fully convolutional network (FCN)
[81]		Liver tumor segmentation	Multi-level deep convolutional network (MDCN) & fractal residual network (FRN)
[82]		Liver and tumor segmentation	3D-DenseUNet-569

Table 1 (continued) Overview of supervised method applications. The last column describes the type of supervised method.

Reference	Abdominal organ	Application	Supervised method
[83]	Kidney	Automatic kidney segmentation from CT images	Deep CNNs (AlexNet and U-Net)
[84]		Renal cortex, renal column, and renal medullar segmentation	Modified AAM, GHT and modified RF
[85]		Renal tumor segmentation and classification	CNN (ScNet)
[86]		Fully automated renal masses (RM) detection and segmentation on CT images	CNN, U-Net-based ensemble learning model
[87]		Automatic segmentation of kidney in US images	Deep CNN and boundary distance regression network
[88]		Measurement of glomerular filtration rate	Modified 3D U-Net
[89]		Renal transplant status assessment	3D CNN
[90]		Automatic renal segmentation in DCE-MR images	3D CNN (3D U-Net)
[91]		Robust contextual segmentation	Parallel FCN networks (foreground, background, and shape FBS Models)
[92]		Automatic kidney segmentation in 3DUS	Deep neural network and weighted fuzzy active shape model
[93]		3D Kidney segmentation from CT images	Random forest (RF) classification
[94]	Gallbladder	Identifying cholelithiasis and classifying gallstones on CT images	Yolo neural network (Yolov3-arch)
[95]	Pancreas	Pancreas segmentation and station recognition system in EUS	Deep convolutional neural network (DCNN): ResNet and UNet++
[96]		Automatic pancreas segmentation on CT images	Deep U-Net
[97]		Pancreas segmentation with uncertain regions of MRI images	2D U-Net
[98]		Pancreas segmentation in CT images	Multiscale residual network (MR_Net)
[99]		Liver guided pancreas segmentation	3D CNN
[100]		Pancreas segmentation in abdominal CT scans	Dense attentional network (DA-Net)
[101]		Pancreas segmentation in 3D CT images	U-Net (SEVoxNet)
[102]		CT pancreas segmentation	Deep Q network (DQN) with deformable U-Net
[103]		Bottom-up approach for pancreas segmentation	Cascaded random forest (RF) and DCNN (*PCNN*)
[104]		Fully automated pancreas segmentation	3D U-Net
[105]		CT pancreas segmentation	TernaryNet
[106]	Spleen	Abdominal spleen segmentation	DNN based on ResNet
[107]		Spleen segmentation	High-level features enhancement network (HLE-Net)
[108]		Automatic spleen segmentation on CT	Multi-Atlas (AGMMCL)
[109]	Multi-organ	Segmentation of thoracic and abdominal organs	Cascaded V-Net
[110]		Annotating abdominal CT images	Deep neural network
[111]		Fully automated segmentation of multiple organs-at-risk (OARs)	Automated deep learning-based abdominal multi-organ segmentation framework (ALAMO – 2D U-Net)
[112]		Multi-organ segmentation	Pyramid input pyramid output feature abstraction network (PIPO-FAN)
[113]		Automated segmentation and volume measurement of the liver and spleen	Deep learning algorithm (DLA)
[114]		Segmentation of 3D multi-organ	OBELISK-Net
[115]		Segmenting 8 abdominal organs	3D U-JAPA-Net

tumor[120], lesion[121] and cyst[122] using supervised segmentation methods. Conze et al.[62] combined standard random forest (RF) and hierarchical multi-scale tree resulting from recursive supervoxel decomposition to segment a hepato-cellular carcinoma liver tumor in dynamic contrast-enhanced CT scans. Li et al.[41] varied the original U-Net by proposing a bottleneck feature supervised (BS) U-Net, which is based on a convolutional neural net-

work (CNN) to segment liver and tumor. Their model entailed an encoding U-Net and a segmentation U-Net. They used the encoding U-Net to train an autoencoder firstly to get label maps encodings, which was used further as additional supervision for the training of the segmented U-Net. Xu et al.[64] segmented liver vessels from contrast enhanced CT images by means of deep neural networks and bootstrapping technology trained on noisy labels.

3.1.2 Kidney

Kidneys are a pair of organs positioned at the rear end of the abdomen and are protected by the rib cage[83]. They are responsible for whole-body homeostasis, regulating acid-base balance, electrolyte concentration, the volume of extracellular fluid, and blood pressure. The kidney consists of four parts with specific functions: renal cortex, renal column, renal medulla, and renal pelvis. These parts are affected by different diseases. For instance, the renal cortex usually suffers kidney tumor, renal column hypertrophy may affect the renal column, medullary cystic kidney disease typically affects the renal medulla, and the renal pelvis mostly suffers transitional cell cancer, and renal pelvis and ureter cancer[84]. The 2018 global cancer statistics reported 400 000 cases of kidney cancer and close to 175 000 deaths due to kidney cancer. However, early and accurate diagnosis of kidney cancer can improve patient′s survival rate. In contrast, late diagnosis and treatment will increase mortality if cancer spreads to surrounding tissues or organs[123]. Hence, kidney segmentation is an imperative step in urology for computer-assisted diagnosis and treatment, and a prerequisite in planning surgery. Accurate segmentation gives information on the structural irregularities in the kidney shape and kidney size measurement, which informs the expert′s analysis of serious clinical conditions, such as carcinoma[83]. Researchers have applied supervised methods to efficiently and accurately segment the kidney′s region of interest over time. Jin et al.[84] combined 3D generalized hough transform (GHT) and 3D active appearance models (AAM) to localize and estimate the thickness of the renal cortex and a modified random forests (RF) method to segment the kidney into the renal cortex, renal column, renal medulla, and renal pelvis components based on the localization phases′ results in clinical 3D CT abdominal images. Pan et al.[85] proposed a multi-task network that involved a segmentation and classification convolutional neural network (SCNet) for renal tumor preoperative assessment. Pan et al.[85] merged two tasks to feed semantic features to the classification network, and the classification results gave segmentation network feedbacks in return. Their results were boosted by 2.8% after they conducted a 2-step segmentation strategy to the segmentation module, and they achieved a 100% classification accuracy and 0.882 segmentation dice coefficient of tumor region. The study of [87] automatically segmented kidneys via subsequent boundary distance regression and a network of pixel classification. Yin et al.[87] extracted high-level image features from ultrasound images using deep neural networks pre-trained for natural image classification. Their extracted features were fed into a boundary distance regression network as input to learn kidney boundary distance maps. Based on their predicted boundary distance maps, they used a pixelwise classification network in an end-to-end learning fashion to classify kidney pixels and non-kidney pixels.

3.1.3 Gallbladder

A normal gallbladder is a pear-shaped abdominal organ anatomically positioned below the liver at the couinaud segments IV and V junction[124]. It contains bile, a digestive fluid from the liver[125]. After a meal, the content of the gallbladder is released into the duodenum, where it emulsifies fats in the food that is partly digested[126]. Gallbladder disease is a widely prevalent internal organs pathological condition[127], which affects a large part of the adult population of developed societies. They manifest commonly as gallstones and gallbladder cancer. The primary cause of admissions to hospitals for gastrointestinal problems affecting almost 15% of the adult population is gallstones. For example, 25 million Americans are affected with gallstones[128], while gallbladder cancer (GBC) accounts for the most common biliary tract malignancy[129] and the 5th top gastrointestinal malignancy globally. That notwithstanding, it is difficult to diagnose GBC and its prognosis is comparatively poor because of the rapid progression characteristics and high mortality rate[130]. However, enhanced early diagnosis could aid on-time treatment and possibly influence patient prognosis[131]. Gallstones form in the gallbladder, bile duct, and liver. It is traditionally categorized into cholesterol stones, black pigment (calcium bilirubinate) stones, brown stones, and mixed stones made up of cholesterol and calcium bilirubinate. However, the classification method depends largely upon the gallstones′ external shape and color, and it does not accurately reflect the cases wherein the gallstones′ internal morphology is different from the external one[132]. Segmentation of the bile duct and gallbladder are of high interest to detect the hepatobiliary and pancreatic systems anomalies and risk factors[17]. Computer technologies development has led to many artificial intelligence-based data mining algorithms being proposed to support experts in clinical stage assessment, decision-making, and prognosis prediction[129]. However, only a few of methods have been presented by the research community to segment the gallbladder[125]. Gloger et al.[17] performed a gallbladder volumetry for both native and secretin-enhanced MR cholangiopancreatography (MRCP) volume data using a fully automated gallbladder segmentation framework. Glover et al.[17] used a 1.5-T MR system to produce native and secretin-enhanced MRCP volume data. They automatically computed 2D characteristic shape features of the gall-

bladder using images of coronal maximum intensity projections (MIP). They generated gallbladder shape space to derive 3D gallbladder shape features and combined them with 2D gallbladder shape features in an SVM approach to detect MRCP volume data′s gallbladder regions. At the same time, they used the region-based level set approach for fine segmentation. They further performed a volumetric analysis for both the native and secretin-enhanced MRCP sequences to calculate the gallbladder volume difference. Pang et al.[94] proposed a Yolov3-arch neural network to identify cholelithiasis and classify gallstones on CT images. Pang et al.[94] trained a Yolo network by first annotating a small amount of CT images that included the spine, liver and gallbladder. They picked out their CT images as a trained set from the trained neural network. Their confidence to detect gallstone was based on the coefficient of the output related to the occurrence probability of the gallstone.

3.1.4 Pancreas

The pancreas is a vital organ of the human body with internal and external secretion functions, but is prone to various diseases[133]. Cancer of the pancreas is the seventh ranked cause of cancer related deaths, with about 432 242 deaths every year and 458 918 new cases[99]. To diagnose and prognos is pancreas diseases, the organ′s identification and segmentation are very essential in the task. Accurate segmentation of the pancreas can give segmentation-based biomarkers, like volumetric measurements and signatures of the 3D shape/surface. However, manually tracing the pancreas boundary slice-by-slice is labor expensive and susceptible to inter-variability and intra-variability. Therefore, robust and automatic segmentation algorithms can aid in processing large-scale image data for relative clinical research[134]. Zhang et al.[99] proposed and validated a location prior guided automatic segmentation of the pancreas using a 3D convolutional neural network. Zhang et al.[99] used a 2D CNN to firstly segment and locate the liver so as to calculate the centroid of the pancreas used to determine its bounding box. After which, they employed a 3D CNN using the pancreas bounding box as input to get the final segmentation. Wang et al.[101] rather segmented the pancreas using a fully 3D cascaded framework by adopting a 3D detection network called PancreasNet to firstly locate the pancreas in CT images. They cropped and down-sampled the pancreas region while they fed the results into a 3D coarse-scale segmentation network known as SEVoxNet-C. Based on their coarse-scale segmentation results, they further refined the pancreas regions and concatenated them as input to the 3D fine-scale segmentation network, also known as SEVoxNet-F. Man et al.[102] employed a deep Q network (DQN) driven technique with deformable U-Net to segment the pancreas accurately while explicitly acting upon the pancreas contextual information and extracting anisotropic features. Farag et al.[103] proposed a bottom-up method to segment the pancreas using image and (deep) patch-level labeling confidences. Farag et al.[103] firstly decomposed CT slice images into a set of boundary-preserving superpixels that were disjointed. With a dense patch labeling, they computed the pancreas class probability maps, then generated image features to classify the superpixels from both intensity and probability information to input into a cascaded random forest. Finally, they enforced a simple spatial connectivity based post-processing.

3.1.5 Spleen

In the lymphatic system, the spleen is the largest organ, it is mostly forgotten by laypeople, yet it is of significant importance to clinicians[135]. The abnormal increase in the spleen size, called splenomegaly, is associated with the destruction of abnormal red blood cells, which is clinically found in patients with liver disease, cancer, and infection[18, 136]. Spleen diseases pose particular challenges since it is not clear characterize healthy subjects from unhealthy subjects. However, the splenic disease has been determined traditionally on simple measurements (width/length) or volumetric estimates. That notwithstanding, such metrics have often failed to characterize splenic disease[135]. In the wake of the traditional approaches′ limitations, modern methods have been widely used to detect anatomical abnormalities with the spleen. Specifically, spleen segmentation is useful for preprocessing for fast diagnosis of blunt splenic injury severity[137], measuring spleen volume, and evaluating anatomical diseases via measurement[106]. Liu et al.[108] proposed a multi-atlas segmentation of the spleen on CT images using an adaptive Gaussian mixture model based on context learning technique called context learning method for performance level estimation (CLSIMPLE). Liu et al.[108] generated a probability map for a target image using the context learning method, while using the Gaussian mixture model (GMM) as the prior in a Bayesian framework. Liu et al.[108] postulated that the CLSIMPLE typically trained a single GMM from the entire set of heterogeneous training atlas. Hence, they opined that the spatial prior estimated maps might not accurately represent the specific target images. Rather than using all training atlases, Liu et al.[108] proposed an adaptive GMM based context learning approach to learn the GMM adaptively while using the training data subsets with the subsets tailored for different target images. They outlined that their training set were adaptively selected based on the similarity between the atlases and the images targeted via cranio-caudal length, which was manually derived from the target image. Liu et al.[108] identified their AGMMCL to accurately segment the spleen by training GMMs adaptively for different target images. Moon et al.[106] devised an automated pipeline for the segmentation of the abdominal spleen. Moon et al.[106] provided an end-to-end synthesized process pipeline that permits users to circumvent any packages installation and

deal locally with intermediate results. Their pipeline did the pre-processing of input data, spleen segmentation using deep learning, reconstruction of 3D using labels generated by matching the segmentation results with dimensions of the original image, which could be used later and for either display or demonstration.

3.2 Multi-organ segmentation

Abdominal multi-organ segmentation of radiology images is essential for clinical applications like computer-aided diagnosis and surgery and radiation therapy[51]. The segmentation of multiple organs relatively assists in targeting and navigation in computer-assisted diagnostic and biomarker measurement systems as nearby organs are used as navigational landmarks[20]. Chen et al.[111] developed an automated deep learning based framework to segment the liver, spleen, pancreas, right kidney, left kidney, stomach, duodenum, small intestine, spinal cord, and vertebral bodies using a 2D U-Net and a structure of a densely connected network with tailored design in the augmentation of data and procedures for training such as deep connection, auxiliary supervision, and multiple views. The model of [111] takes in as input multi-slice MR images and produces the segmentation results as output. Fang and Yan[112] employed a multi-scale deep neural network feature abstraction to segment the liver, spleen, and kidney over partially labeled datasets. Fang and Yan[112] further proposed a new network architecture to abstract multi-scale features integrated into a U-shape pyramid structure, pyramid input, and feature analysis. They introduced an equal convolutional depth technique to bridge the semantic gap caused by the direct merging features from the different scales. Fang and Yan[112] then employed a deep supervision technique to refine the outcome in different scales. They designed an adaptive weighting layer to incorporate the outcomes in an automatic fashion so as to fully leverage their segmentation features from all the scales. Fang and Yan[112] harnessed a unified training mechanism that allowed a multi-scale deep neural network to train their datasets. Ahn et al.[113] segmented and measured the volume of the liver and spleen using a deep learning algorithm trained with the development of portal venous computed tomography images. Kustner et al.[138] implemented and validated automated semantic 3D liver and spleen segmentation on multi-contrast MR data using DCNet (CNN) compared against a random forest segmentation. Gibson et al.[20] proposed a deep learning-based algorithm (dense VNet) to automatically segment the pancreas, stomach, spleen, esophagus, liver, gallbladder, left kidney and duodenum on abdominal CT images.

In this section, we reviewed single and multi-abdominal organs, their significance in the anatomical structure, their morbidity and mortality rates, and some supervised techniques used by some researchers for single and multi-abdominal organs segmentation.

4 Applications based on semi-supervised segmentation method

This section provides a summary of semi-supervised abdominal segmentation applications for single abdominal organs and multi abdominal organs.

4.1 Single abdominal organ segmentation

In this section, we present an overview of the following single abdominal organs: liver, kidney, gallbladder, pancreas, and spleen. Some research works based on semi-supervised segmentation methods are outlined. Table 2 also gives an overview of the semi-supervised segmentation method applications as regards the specified organs.

4.1.1 Liver

Zheng et al.[139] presented a semi-supervised liver segmentation mechanism built on an adversarial learning model, which incorporated prior knowledge with deep learning to enhance the accuracy of the segmentation. They used both annotated and unannotated images to train the semi-supervised adversarial learning model. Zheng et al.[139] extracted the probabilistic atlas of the liver, defined a deep atlas prior (DAP) loss, and proposed a Bayesian loss. Based on the principle of the Bayesian model, which involves a likelihood and a prior, they combined the DAP loss and focal loss. Borga et al.[29] introduced an atlas-based segmentation and validated their approach on liver segmentation in abdominal magnetic resonance images. Borga et al.[29] adapted a semi-supervised approach of a graph recounting a manifold of anatomical disparities of whole-body images while using unlabeled data to identify a path with slight deformations from the labeled atlas to the targeted image. Borga et al.[29] proposed increasing the dataset numbers and segmentation of other anatomical structures for future studies, but they identify that they have not evaluated their method on other organs or image modalities other than MR as the limitation of their study. Liao et al.[143] developed a density peak (DP) clustering, graph cuts, and border marching method for automatic liver segmentation from CT volumes. They segmented an initial slice by density peak clustering. They then developed an intensity model and a PCA-based regional appearance model based on pixel-wise and patch-wise features to enhance the contrast between liver and background. Liao et al.[143] integrated the models together with the location constraints estimated iteratively into graph cuts so as to segment the liver in every single slice automatically. Liao et al.[143] finally increased the segmentation accuracy using a vessel compensation method based on border marching. Huang et al.[144] presented a fully automatic procedure that employs modified graph cuts and feature detection for the accurate and fast segmentation of the liver. Huang et al.[144] automatically determined the initial slice and

Table 2 Overview of semi-supervised segmentation method applications. The last column describes the type of semi-supervised method used.

Reference	Abdominal organ	Application	Semi-supervised method
[139]	Liver	Liver segmentation	Semi-supervised adversarial learning model (Segmentation network and discriminator network)
[140]		Automatic 3D liver location and segmentation	Graph cut and CNN
[141]		Extracting the liver from CT images	Graph cut
[142]		Automatic liver segmentation on volumetric CT images	Supervoxel-based graph cuts
[143]		Automatic liver segmentation from abdominal CT volumes	Graph cuts and border marching
[144]		Fully automatic liver segmentation in CT images	Modified graph cuts
[145]	Kidney	Precise estimation of renal vascular dominant regions	Tensor-cut, spatially aware FCN, and voronoi diagrams
[146]		Automatic renal segmentation for MR urography	3D-GraphCut and random forests
[147]		Segmenting kidneys in 2D US images	Graph cuts
[148]	Pancreas	Semi-supervised medical image segmentation and domain adaptation	Uncertainty-aware multi-view co-training (UMCT)
[149]		Medical image segmentation	Semi-supervised task-driven data augmentation method
[150]		3D semi-supervised learning	UMCT
[151]		Organ segmentation refinement	Uncertainty-based graph convolutional networks
[152]	Spleen	Splenomegaly segmentation	Co-learning and DCNN
[153]	Multi-organ	Unified multi-organ segmentation	Co-training weight-averaged models
[154]		Multiple-organ segmentation	Graph cuts
[155]		Automatic multiorgan segmentation for 3D radiological images	Graph cuts

seeds of graph cuts using an intensity-based mechanism with prior position information. They enhanced the weak boundaries of soft organs and prevented over-segmentation by proposing a contrast term founded on the similarities and variances of local organs across multi-slices. Huang et al.[144] then integrated the contrast term into the graph cuts for the automatic segmentation of the slice and prevented leakage by using the neighboring slices of the patient-specific intensity and shape constraints. Finally, they proposed a feature detection method that depended on vessel anatomical information to remove the neighboring inferior vena cava with similar intensities.

4.1.2 Kidney

Zheng et al.[147] segmented kidneys in US images by proposing a dynamic graph-cuts (GC) based segmentation method with multiple feature maps integrated. Zheng et al.[147] built a graph of image pixels with close proximity to the kidney boundary and not a graph of the whole image. This was meant to handle kidney images with large appearance variations and to enhance the efficiency of computation. They further made the segmentation of the kidney robust to weak boundaries by adopting localized regional information to measure resemblance between image pixels for edge weights computation to construct the graph of image pixels. They dynamically updated the localized graph, and the graph-cuts based segmentation looped until convergence. Wang et al.[145] proposed a fully automatic segmentation method that integrated a neural network and tensor-based graph-cut methods to precisely estimate the renal vascular dominant region using a voronoi diagram. Wang et al.[145] firstly used a CNN to localize the regions of the kidney and with tensor-based graph-cut method they extracted tiny renal arteries. They then generated a voronoi diagram to approximate the dominant regions of the renal arteries based on the kidney and renal arteries segmented. Yoruk et al.[146] presented an automatic renal segmentation method that used spatial and temporal domains to fully segment the kidney and renal cortex. Yoruk et al.[146] built a heuristic approach to locate kidneys with the help of the medulla as a target, they revised a GrabCut algorithm to function in 3D, and incorporated the modified GrabCut algorithm to the time resolved magnetic resonance imaging data using principal component analysis dimensionality reduction, and finally trained an RF classifier to segment the renal tissue into cortex, medulla, and the collecting system.

4.1.3 Gallbladder

Saito et al.[156] proposed a fast approximation for optimization. They evaluated their proposed method in a gallbladder segmentation context from a non-contrast CT volume. Saito et al.[156] used a branch-and-bound method

to simultaneously optimize the segmentation, shape, and location priors after they spatially standardize and estimate the posterior probability of the target organ. Saito et al.[156] achieved a fast approximation by compounding sampling in the eigenshape space to cut down the number of shape priors and efficient computational method for assessing the lower bound. The proposed joint optimization of the segmentation, shape, and location priors by [156] proved to be effective in the segmentation of the gallbladder with high computational efficiency.

4.1.4 Pancreas

Xia et al.[148] proposed an uncertainty-aware multi-view co-training framework that leveraged on unlabeled data for better performance. Xia et al.[148] firstly rotated and permuted their 3D volumes into more than one view and trained a 3D deep network on every one of the views. They then applied co-training by implementing multiple view consistency on unlabeled data, where an uncertainty estimation of every one of the views was exploited to attain accurate labeling. Chaitanya et al.[149] proposed a method based on semi-supervised task-driven data augmentation to address the challenge of realizing a robust segmentation in a training setting with limited data. Their proposed method′s generator intensity and shape disparities used two classes of transformations: addictive intensity transformations and deformation fields. Both transformations used a semi-supervised framework to optimize labeled and unlabeled examples. Their proposed model was evaluated on three different publicly available datasets for segmentation, including the pancreas. Xia et al.[150] proposed an uncertainty-aware multi-view co-training (UMCT) model for 3D data to segment pancreas. Xia et al.[150] exploited 3D multi-viewpoint consistency by generating varied views while rotating or permuting the 3D data using the asymmetrical 3D kernels to trigger in different sub-networks diversified features. They further estimated the reliability of every view′s prediction with Bayesian deep learning while proposing an uncertainty-weighted label fusion (ULF) mechanism. Xia et al.[150] obtained more accurate pseudo labels for every view, which they used as a signal for supervision for unlabeled data after propagating through the ULF module. Soberanis-mukul et al.[151] employed a technique of segmentation refinement which depended on uncertainty analysis and networks of graph convolution. Soberanis-mukul et al.[151] formulated a semi-supervised graph learning problem that was solved by training a graph convolutional network which employed the uncertainty levels of the convolutional network in a specific input volume. Soberanis-mukul et al.[151] tested their approach by refining the initial output of a 2D U-Net. They further validated their framework with two different datasets, the National Institutes of Health (NIH) pancreas dataset and the spleen dataset of the medical segmentation decathlon.

4.1.5 Spleen

Huo et al.[18] proposed and used multi-atlas segmentation for clinical magnetic resonance imaging spleen segmentation for splenomegaly. Huo et al.[18] first used an automated segmentation technique that employed a selective and iterative method for performance level estimation (SIMPLE) atlas selection to rectify the concerns of inhomogeneity for clinical splenomegaly magnetic resonance imaging. Then, to further control outliers, Huo et al.[18] proposed semi-automated craniocaudal spleen length-based SIMPLE atlas segmentation (L-SIMPLE) to fuse a spatial prior in a Bayesian fashion and guide iterative atlas selection. Huo et al.[18], lastly, employed graph cuts refinement to achieve the final segmentation from the probability maps from multi-atlas segmentation (MAS). Tang et al.[152] designed a co-learning strategy to train a deep network from heterogeneously labeled scans; hence, they proposed a new method of deep convolutional neural network (DCNN) that integrated heterogeneous multi-resource labeled cohorts for the segmentation of splenomegaly. Tang et al.[152] introduced a loss function based on the Dice similarity coefficient to learn multi-organ information adaptively from varied resources. They employed three cohorts in their experiments: Their first cohort had only splenomegaly labels, while the second, a training cohort, had 15 distinct anatomical labels with spleens with normal spleens. Tang et al.[152] used as a testing cohort, a distinct, independent cohort that involved 19 splenomegaly CT scans with labeled spleens. Their new DCNN achieved the highest median Dice similarity coefficient value compared to multi-atlas, SS-Net (with only spleen labels), and U-Net segmentation with multi-organ training. Huo et al.[136] proposed a network of splenomegaly segmentation which leveraged on the segmentation performance by using large convolutional kernels in the skip connection layers for the spleen that was large. They further employed adversarial networks to discriminate the segmentation performance for training that was end-to-end, and finally they improved their splenomegaly segmentation using 2D+ multi-view training. Huo et al.[157] proposed frameworks based on multi-atlas segmentation to segment MRI spleen for splenomegaly. Huo et al.[157] introduced an automated approach based on a selective and iterative method to interactively select a subset of atlases for the performance level estimation (SIMPLE) approach. They also introduced a spatial prior to guide the iterative atlas selection by proposing a semi-automated craniocaudal length based SIMPLE atlas selection to control the outliers.

4.2 Multi-organ segmentation

Huang et al.[153] co-trained weight-averaged models for learning from few-organ datasets, a unified multi-organ segmentation network. Huang et al.[153] trained collaboratively two networks and allowed both networks to teach one another on un-annotated organs. They adopted the weighted-average models to alleviate the noisy teaching supervisions that existed with the networks in order to generate dependable soft labels. Huang et al.[153] further utilized a region mask to selectively apply the consistent constraint on regions of the un-annotated organ that

needed collaborative teaching, which enhanced the performance. Experiments conducted by Huang et al. on four public datasets identified their framework to better utilize few-organ data and realized superior performance with less computational cost on public datasets. Zhou et al.[51] designed a deep multi-planar co-training (DMPCT) for multi-organ segmentation by exploiting multi-planar information to produce pseudo-labels for 3D CT volumes that are unlabeled. The DMPCT framework is a systematic EM-like semi-supervised learning model consisting of the following models; teacher, multi-planar fusion module, and a student model. Zhou et al.[51] trained the teacher model from more than one plane distinctly in a slice-by-slice approach with annotations, the DMPCT enjoyed extra benefits of continuously producing more dependable pseudo-labels by the multi-planar fusion system, few helped train the student model with massive unlabeled data. Zhou et al.[51] introduced co-training as multiple segmentation networks that corresponded to varied planes in the teacher and student models. They did it so that the networks could be trained concurrently in their unified framework and benefit from one another. Takaoka et al.[154] introduced a higher-precision technique to segment multiple organs with the aid of graph cuts within medical images like CT-scanned images. Takaoka et al.[154] advanced supervoxels instead of voxels as the segmentation units, i.e., the graphical model′s nodes, and they designed the energy function that minimized accordingly. They then used the SLIC supervoxel algorithm and evaluated the performance of their segmentation algorithm by energy minimization likening to the ground truth. Kéchichian et al.[155] designed a method that automatically segments multiorgan for 3D radiological images of varied anatomical components and modalities. Kéchichian et al.[155] followed the Bayesian model and advanced location and intensity prospects of structures together with a prior distribution of their corresponding spatial configuration. They defined the location likelihoods by target-specific probabilistic atlases created by recording atlases to the target in shrinking frames with the aid of a fast SURF-based registration technique that projected a homothetic transformation. Kéchichian et al.[155] used confidence regions of probabilistic atlases to obtain the target-specific intensity possibilities. They derived the spatial prior from shortest-path constraints spelt out on the adjacency graph of structures. Kéchichian et al.[155] defined an energy function using the likelihoods and spatial prior, optimized by a multilabel Graph cut method to derive the multiorgan segmentation.

In this section, we covered some works by the research community on semi-supervised segmentation applications for single and multi-abdominal organs.

5 Datasets and evaluation

This section outlines abdominal organ datasets and the web source to the datasets.

5.1 Datasets

One of the biggest producers of data is the medical domain. Today clinical practice and medical research produce vast numbers of images of high dimension[155]. In 2011, 30% of the world′s storage was estimated to contain medical images, which showed the enormous and often miscalculated amount of data generated in medical institutions. Presently, these images are primarily used for single patient treatment and only in restricted form across groups of patients or for education. This secondary use of the data presents some benefits, and the extracted content directly from the images is complementary to clinical data that is structured and free text that is mostly used in medical decision support[158]. Image segmentation, as a critical stage in medical image analysis, advances on models that aids in the visualization and extraction of ROI for supporting medical decisions. In order to build a segmentation model that is reliable, a precondition is the availability of a large quantity of labeled data for training[25], and current unconventional segmentation models still need a large, representative, and high quality annotated datasets[159]. However, perfectly-sized and carefully-labeled datasets are rare for training an image segmentation model. Usually, datasets of medical images are small, this is because it is extremely time-consuming to annotate and expert knowledge is also required[139]. Hence, this limits the medical image segmentation datasets to scarce, weak, noisy, image-level annotated data available for training[159]. Though the medical domain is producing large volumes of data, the supervised machine learning algorithms′ challenge is the lack of annotated data[13, 46]. The supervised deep learning method also faces the same challenge[159] and even requires large labeled training set to achieve high accuracy[51] in their training[11]. On the other hand, semi-supervised machine learning algorithms for medical image segmentation can make effective use of data that is unannotated[139].

Several datasets that are commonly used for abdominal organ segmentation are publicly available, and they are manually labeled or annotated atlases devoid of basic information about patients[30], while private datasets are also mostly created by researchers by collecting data from volunteers[159], patients or hospitals[160] after satisfying ethical and or patient consent[161] to complement their research works when the need arises. The following abdominal organ specific datasets are publicly available: for liver – Sliver07 dataset from the Medical Image Computing and Computer Assisted Intervention Society MICCAI liver segmentation challenge (MICCAI-Sliver07), 3Dircadb dataset from Research Institute against Digestive Cancer (3DIRCADB), the MIDAS liver tumor dataset from National Library of Medicines Imaging Methods Assessment and Reporting (IMAR) project[33], Liver Tumor Segmentation Challenge (ListS-ISBI2017)[66], kidney – MICCAI

2019 Kidney Tumor Segmentation Challenge (KiTS19)[123], pancreas – NIH[98] from the National Institutes of Health Clinical Center, BTCV[100] from Beyond the Cranial Vault, ISICDM from the challenge on the 2019 International Symposium on Image Computing and Digital Medicine[99], spleen – Spleen segmentation dataset[112], multi-organ – VISCERAL, and TCIA[114] from The Cancer Imaging Archive. These datasets come in a CT, MRI, or US modalities. Datasets that are publicly available are very important for the community of researchers. However, it is also critical to compare the pros and cons of segmentation methods, this is because it is more meaningful to correlate the accuracy of distinct segmentation methods using the same dataset.

The MICCAI-Sliver07 dataset consists of 30 CT scans made up of 20 training data with matching ground truth and 10 testing data without ground truth. Datasets in this database are pathological and made up of tumors, metastases and cysts of varied sizes[162]. All the volumes of the MICCAI-Sliver07 dataset have an in-plane resolution of 512 × 512 pixels. The inner-slice pixel spacing ranges from 0.576 2 mm to 0.812 5 mm, and the slice thickness also ranges from 0.7 mm to 5.0 mm. The number of slices in every case ranges from 64 to 394[163].

The LiTS dataset consists of 200 3D liver CT scans from more than one clinic. The dataset involves images of varying spatial resolution and fields-of-view. The images have axial slices of 512 × 512, with 0.45–5.0 mm slice spacing, an in-plane resolution of 0.60–0.98 mm. The LiTS dataset is divided into 130 CT scans in training and 30 CT scans in testing[36].

The ISICDM dataset is from the 2019 International Symposium on Image Computing and Digital Medicine Challenge. It comprises of liver data that has 24 subjects with manually delineated liver annotations, varied image sizes and fixed resolution of $1 \times 1 \times 5\,\text{mm}^3$, and pancreas data that involves 36 training and 18 testing images, with the ground truth segmentation of the images for testing hidden during the challenge. "Thick" and "thin" are the two subsets of this dataset with a 5 mm and 1 mm spacing respectively along the axial plane[99].

The 3DIRCADB dataset comprises 20 venous phases enhanced CT scans of 10 men and 10 women, 15 of the volumes have hepatic tumors in the liver, i.e., 75% of the instances. The level of size and number of tumor lesions and contrast enhancement differentiates the CT volumes substantially[36]. The 20 folders represent 20 different patients and every patient has more than 120 image slices. Every image has a resolution of 512 × 512 width and height, and the number of slices for each patient is between 74 and 260[70].

The MIDAS dataset contains a collection of biomedical multimodal images available in DICOM format and consists of metadata images. The dataset supports 20 types of varied format images corresponding to medical and non-medical images. Researchers can use the MIDAS database in the area of biomedical multimodal imaging which involves image segmentation, computer-aided design (CAD) methods, registration, and techniques for fusion[164].

The KiTS19 dataset consists of a collection of multiphase CT imaging, segmentation masks, and the comprehensive clinical results for 210 patients. The KiTS19 dataset was collected between 2010 and 2018 from varied centers for kidney tumor segmentation. The KiTS19 volume slice thickness ranges from 2–5 mm, and the images have a spatial size of 510 × 510 pixels with different number of depth slices of 21–600 for every patient[165].

The NIH pancreas segmentation dataset consists of 82 contrast-enhanced abdominal CT scans with a volume size of 512 × 512 × D, where the D belongs to 181 and 466. The volumes spatial resolutions height and weight are between 0.5–1.0 mm and 1.0 mm depth[36].

The BTCV dataset consists of abdominal CT scans obtained at the Vanderbilt University Medical Center from cancer patients with metastatic liver or post-operative ventral hernia patients. The images voxel sizes are from 0.6–0.9 mm in the left-right axis and anterior-posterior, and 0.5–5.0 mm in the inferior-superior axis. The anterior-posterior fields of view are from 172–318 mm, 246–367 mm for the left-right axis, and 138–283 mm for the inferior-superior axis realized from manual cropping the rib-cage[36].

The Medical Segmentation Decathlon (MSD) spleen dataset consists of CT volume images from patients who were undergoing treatment of chemotherapy for liver metastases at Memorial Sloan Kettering Cancer Center and formerly reported. The CT scans are made up of 61 portal venous phases were added with a CT reconstruction and acquisition parameters similar to the Task08_HepaticVessel dataset as specified in [166].

The VISCERAL dataset contains four modalities: CT and MR scans of the whole body, CECT scans of the entire trunk, and T1 contrast-enhanced MR scans of the abdomen (Kidney, urinary bladder, gallbladder, spleen, liver, and pancreas[167]). Every modality specified has 30 clinical scans (20 scans for training dataset and 10 scans for test dataset)[168].

The Cancer Imaging Archive (TCIA) dataset consists of radiology images depicting the data of about 37 568 subjects collected and it is the repository for cancer imaging and related information for the US National Cancer Institute. The TCIA dataset is organized into tumor type collections with other collections, which includes analytic results or clinical data[169]. In addition, the TCIA multilabel dataset consists of labels of spleen, kidney, esophagus, pancreas, gallbladder, stomach, liver, and duodenum[114].

For more information on abdominal organ segmentation datasets, refer to [167] and Table 3 for the web source to the datasets, and [170] for the medical image segmentation datasets limitations.

Table 3 Publicly available abdominal organ(s) datasets

Organ	Dataset	Web source
Liver	LiTS	https://competitions.codalab.org/competitions/17094
Liver	Sliver07	https://www.sliver07.org
Liver	3Dircadb	https://www.ircad.fr/research/3d-ircadb-01
Liver	MIDAS	https://www.insight-journal.org/midas/
Liver	ISICDM	http://www.imagecomputing.org/2019/challenge.html
Pancreas	NIH	https://wiki.cancerimagingarchive.net/display/Public/Pancreas-CT
Kidney	KiTS19	https://kits19.grand-challenge.org/
Spleen	MSD-spleen	http://medicaldecathlon.com
Multi-organ	BTCV	https://www.synapse.org/#!Synapse:syn3193805/wiki/217789
Multi-organ	VICERAL	https://www.smir.ch/VISCERAL/Start
Multi-organ	TCIA	https://www.cancerimagingarchive.net

5.2 Evaluation

Diverse evaluation metrics are used to analyze the performance of abdominal organ segmentation methods. The accuracy of the segmentation algorithms often proposed by researchers is evaluated with three common metrics: volume-based, surface distance-based and clinical performance metrics[11]. These metrics are used to verify the performance segmentation methods between the ground truth and test results[66]. Dice similarity coefficient (DSC), Jaccard (JAC) index, relative volume difference (RVD), and F1-score are the most common metrics used in the referenced literature and they are calculated using (1)–(5).

$$DSC = 2 \times |R_1 \cap R_2| / (|R_1| + |R_2|) \tag{1}$$

$$JAC = (|R_1 \cap R_2|) / (|R_1 \cup R_2|) \tag{2}$$

$$RVD\,((A/B) - 1) \times 100 \tag{3}$$

$$F_1 = 2TP/(2TP + FP + FN) \tag{4}$$

$$Accuracy = (TP + TN) / (TP + FN + TN + FP) \tag{5}$$

where R_1 indicates a ground truth region and R_2 a segmentation result region[30]. A and B denote the total volume of the segmentation region and total volume of the ground truth respectively[33]. TP represents True Positive – number of pixels/voxels correctly classified, TN represents True Negative – number of background pixels/voxels correctly classified, FP represents False Positive – number of pixels/voxels wrongly classified, and FN represents False Negative – number of background pixels/voxels wrongly classified[145, 171].

DSC is also known as Sorensen-Dice index (SDI), Sorensen Index (SI)[172]. DSC represents an algorithm's overall performance in correctly including the ROI pixels inside the segmentation. It is considered superior and noted to segment boundaries because it only evaluates labeled pixels correctly. DSC is additionally often used to measure system performance repeatability through cross-validation[173]. There is no overlap between the segmented region and the ground truth when a value of 0 is obtained, but a value of 1 represents perfect segmentation. Jaccard (JAC) index is mostly excluded in instances where DSC is reported since it provides the same ranking[33].

JAC is also known as Intersection-over Union (IoU). It calculates the ratio of the area of the overlap between the segmentation predicted and the segmentation of the ground truth to the area of union between the segmentation predicted and the ground truth segmentation. JAC and DSC are similar as they are monotonic in one another or correlated positively. However, what differentiates JAC from DSC is that, JAC penalizes instances of results that are incorrect more than the DSC. Hence, JAC or DSC can be used for segmentation validation instead of using both[173].

RVD non-symmetrically calculates the results and reference volumes difference and represents that both volume sizes are equal if a value 0 is recorded, but this does not imply that the segmentation results and the ground truth masks are identical. RVD metric reveals if a method inclines to over– (positive number) or under– (negative number) segment the image[79].

F_1-score, also known as Boundary F_1 (BF) specifies the harmonic mean of precision (positive predictive value) and recall (true-positive rate or sensitivity)[146]. It is convenient for contour or boundary matching between predicted segmentation and ground truth segmentation. It is also known as the DSC[173].

Table 4 gives a summary of abdominal organs segmented using the supervised method, the used datasets, and their dice score. Table 5 gives a summary of abdominal organs segmented using the semi-supervised method, the used datasets, and their evaluation score. From the refer-

Table 4 Summary of abdominal organs segmented using supervised method: The reference, organ, modality, datasets used, data size, application and dice score.

Reference	Abdominal organ	Modalities	Dataset	Data size	Segmentation application	Dice score (%)
[63]	Liver	CT	Public Dataset, MICCAI-Sliver07, 3DIRCADB & Annotated Subjects (Clinical experts)	160	Liver	96.00
[65]		CT	Public 3DIRCADB & Private	120	Normal liver tissue	95.70
					Tumor tissue	96.10
[66]		CT	LiTS-ISBI2017	130	Liver-tumor Liver	89.72 98.51
			3DIRCADB	–	Liver-tumor Liver	68.14 96.01
[67]		CT	LiTS	–	Liver-tumor	96.10
[62]		DCE-CT	8 Examinations	48	Parenchyma Active Tumoral	95.50 80.40 91.00
[41]		CT	LiTS		Liver Tumor	96.10 56.90
[64]		CT	Local Hospital, 3DIRCADb	56	Liver vessel	68.70
[82]		CT	LiTS-2017	201	Liver Tumor	96.20 69.60
[174]		CT	R Adams Cowley Shock Trauma Left (STC) &ryder Trauma Left (RTC)	73	Whole liver volume	95.00
[175]		CT	LiTS-2017	201	Liver	94.24
[88]	Kidney	SPECT/CT	Tc-99m DTPA kidney SPECT/CT Data	393	Renal parenchyma	89.00
[89]		DW-MRI	DW-MRI Data	32	Kidney	91.00
[90]		DCE-MRI	Hospital	30	Normal	91.40
					Abnormal	83.60
[91]		US	Population1	108	Kidney	77.24
			Population2	123	Kidney	72.83
[93]		CT	Private	60	Kidney	97.30
[85]		CT	Jiangsu Province Hospital	131	Renal	88.20
[123]		CT	KiTS19	300	Kidney	96.74
[17]	Gallbladder	MRCP	SHIP	–	Tumor	84.54
					Native MRCP	92.00
					Secretin-enhanced MRCP	90.00
[96]	Pancreas	CT	NIH-CT	82	Pancreas	78.90
[97]		MRI	Changhai Hospital	20	Uncertain regions	73.88
		CT	NIH-CT	82	Uncertain regions	84.37
[98]		CT	NIH-CT	82	pancreas	87.57
[100]		CT	NIH Pancreas, BTCV	129	Pancreas	81.39
[103]		CT	NIH	80	Pancreas	70.70
[104]		CT	NIH-CT	82	Pancreas	85.99
[101]		CT	NIH	82	Pancreas	85.93
[99]		CT	ISICDM	78	Pancreas	80.71
[102]		CT	NIH	82	Pancreas	86.93
[105]		CT	NIH-CT	82	Pancreas	71.00
[107]	Spleen	CT	Memorial Sloan Kettering Cancer Left	41	Spleen	96.40
[109]	Multi-organ	CT	Multi-atlas Labeling Beyond the Cranial Vault (BCTV)	30	Multi-organs	78.76

Table 4 (continued) Summary of abdominal organs segmented using supervised method: The reference, organ, modality, datasets used, data size, application and dice score.

Reference	Abdominal organ	Modalities	Dataset	Data size	Segmentation application	Dice score (%)
[110]		CT	Dual-phase CT Datasets	236	Multi-organs	89.40
[111]		MRI	T1-VIBE	102	Multi-organs	90.00
[112]		CT	LiTS KiTS Spleen Seg. dataset BTCV	201 300 – 47	Multi-organs	94.40
[113]		CT	Dataset-1	150	Liver Spleen	97.30 97.40
			Dataset-2	50	Liver (External) Spleen (External) Liver (Internal) Spleen (Internal)	98.20 96.90 98.30 96.80
[20]		CT	Pancreas -CT & BTCV	90	Spleen L. Kidney Gallbladder Esophagus Liver Stomach Pancreas Duodenum	95.00 93.00 73.00 71.00 95.00 87.00 75.00 63.00
[114]		CT	VISCERAL	10	7 organs	82.27
			TCIA	43	8 organs	79.03

enced literature, DSC is the most frequently used evaluation index for the abdominal organ segmentation accuracy measurement since its calculation is most convenient, and the value is larger as compared to JAC for the same two images. This indicates that the DSC has a much better effect of calibration[30].

Section 5 reviewed medical image datasets, the source and properties of publicly available datasets for the liver, kidney, pancreas, gallbladder, spleen, and multi-abdominal organs, and the metrics used for the evaluation of the performance of abdominal organ segmentation methods based on ground truth and test results.

6 Discussions and future directions

In the previous sections, we reviewed supervised and semi-supervised abdominal organ segmentation methods with respect to single and multi-organs, datasets, and evaluation from selected papers. This section focuses on discussing literature, existing challenges, and future prospects for abdominal organ segmentation.

6.1 Discussions

Various abdominal organs have been discussed with respect to supervised and semi-supervised methods used in the process of segmentation throughout this paper. The publications on supervised and semi-supervised methods for abdominal organ segmentation are illustrated in Figs. 1–4. The results are collected by using the following search terms: "kidney segmentation", "liver segmentation", "gallbladder segmentation", "spleen segmentation", "pancreas segmentation", "multi-organ segmentation" in the title on Web of Science core collection.

From Fig. 1 and the literature reviewed, current state-of-the-art supervised segmentation methods are based on deep learning techniques. As compared to the conventional and atlas methods, deep learning methods have achieved much better performance recently[73]. Since it is successful in real world applications, it also provides good accuracy, that notwithstanding it is projected as a prime method in the medical field for future applications[36]. Deep learning approaches, such as U-Net, FCN, DNN, among others, have shown remarkable potential in automatic segmentation[177] of abdominal organ images. Hence, they have efficiently been proposed for the segmentation of abdominal organs.

Also, from Fig. 2 and the literature reviewed, it can be deduced that current state-of-the-art methods of semi-supervised segmentation regarding abdominal organs are essentially based on graph and self-training techniques. There has been an increasing interest in graph techniques due to their convexity, scalability and effectiveness in application. A graph-based SSL convexity ensures easier attainment of a local solution by the optimization problems than the general case. Graph-based SSL is scalable due to its flexibility in dealing with big data large-scale datasets. Graph-based semi-supervised learning methods seek to learn the function predicted for the labels of unlabeled samples by exploiting the information of the label dependency reflected by the label information

Table 5 Summary of abdominal organs segmented using the semi-supervised method: The modality, datasets used, data size, application, evaluation type and evaluation score.

Reference	Abdominal organ	Modalities	Dataset	Data size	Segmentation application	Evaluation type	Evaluation score (%)
[140]	Liver	CT	MICCAI-Sliver07	78	Liver	RVD	2.7
			3DIRCABD		Liver	RVD	0.97
[142]		CT	MICCAI-Sliver07	30	Liver	RVD	4.16
[143]		CT	MICCAI-Sliver07 & XHCSU14 (Local Database)	40	Liver	RVD	− 0.1
[144]		CT	Sliver07,	20	Liver	RVD	− 0.6
			3DIRCADB & Local Clinical Datasets	20	Liver	RVD	0.7
[29]		MRI	Philips Health Care & GE Healthcare Global Diagnostic Imaging	36	Liver	SI	97.0
[163]		CT	XHCSU14	20	Liver	Dice	97.3
			MICCAI-Sliver07	–	Liver	Dice	97.2
[145]	Kidney	CT	Kidney Dataset	27	Kidney	Dice	95
				8	Renal artery	Dice	80
[146]		DEC-MRI	Group 1, Group 2, Group 3	26	Renal cortex	F1	0.86
			DCE-MRI Dataset	45	Renal	F1	0.93
[147]		US	Clinical Kidney US images	85	Kidney	Dice	95.81
[156]	Gallbladder	CT	Patients	27	Gallbladder	Jaccard Index	0.623
[148]	Pancreas	CT	NIH	82	Pancreas	(10% labeled training cases)	
						Dice	78.77
					Pancreas	(20% labeled training cases)	
						Dice	81.18
[151]		CT	NIH	65	Pancreas	Dice	77.8
[150]		CT	NIH	82	Pancreas	(10% labeled training cases)	
						Dice of 2 views Dice of 3 views Dice of 6 views	75.63 77.55 77.87
						(20% labeled training cases)	
						Dice of 2 views Dice of 3 views Dice of 6 views	79.77 80.14 80.35
[176]		CT	NIH	82	Pancreas	Dice	82.4
		MRI	UFL-MRI	79	Pancreas	Dice	80.5
[152]	Spleen	CT	ImageVU	100	Normal	Dice	94.0
				117	Splenomegaly		
[136]		MRI	T1w & T2w	60	Splenomegaly	Dice	94.10
[157]		MRI	T1w/T2w	55	Splenomegaly	Dice	88.0
[153]	Multi-organs	CT	MOBA	90	Multi-organs	Dice	83.60
[51]		CT	Newly Collected Large Dataset	310	Multi-Organ	Dice	77.94
[154]		CT	–	24	Multi-organs	Jaccard index	80.69

available[56]. Self-training is gaining attention since it does not need any particular assumption and also allows learning tasks to be trained on inadequately labeled training data. This shows impressive outcomes in SSL[178]. Self-

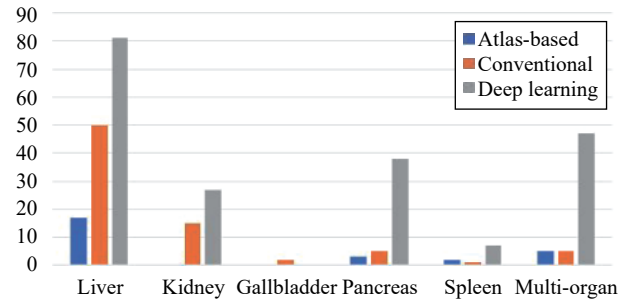

Fig. 1 The number of supervised segmentation methods: Atlas, conventional, and deep learning publications between 2016 and 2021 in Web of Science Core Collection as of March 23, 2021.

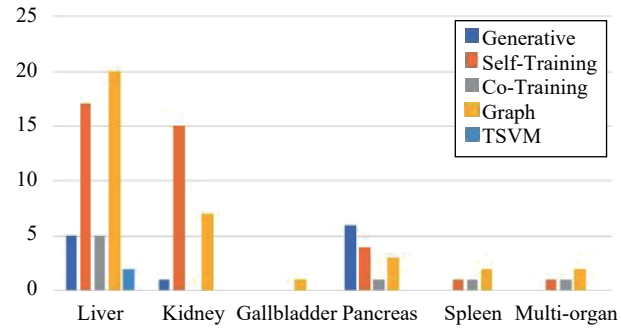

Fig. 2 The number of semi-supervised segmentation methods: Generative, self-training, co-training, graph, and TSVM publications between 2016 and 2021 in Web of Science Core Collection as of March 23, 2021

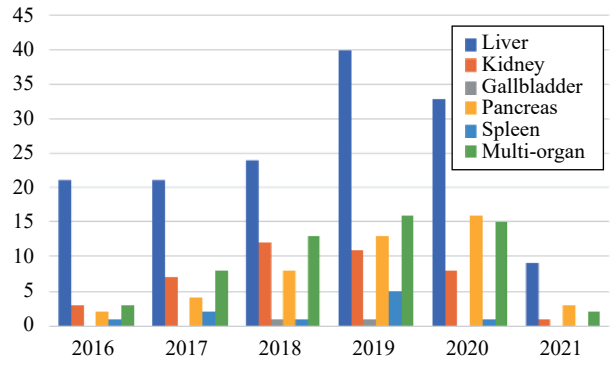

Fig. 3 The number of single and multi-abdominal organ supervised segmentation method publications between 2016 and 2021 in Web of Science Core Collection as of March 23, 2021.

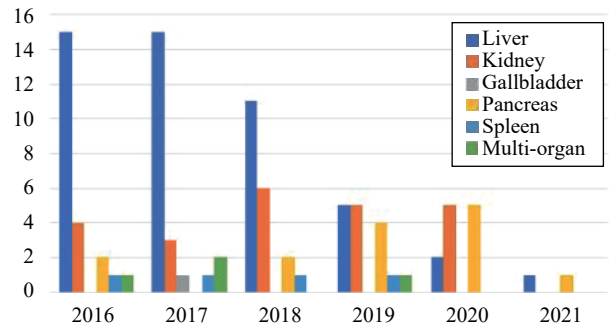

Fig. 4 The number of single and multi-abdominal organ semi-supervised segmentation method publication between 2016 and 2021 in Web of Science Core Collection as of March 23, 2021

training techniques can also be used with any classifier, and it is one of the SSL's most straightforward approaches[26].

From Figs. 3 and 4, more supervised methods have been used to segment abdominal organs as compared to the semi-supervised methods. In the past years, researchers have sought to attain more accurate segmentation results within the framework of supervised machine learning due to the significant focus on the deep learning network's automatic feature extraction instead of the manual feature extraction and the substantial improvement in computational power. Moreover, the supervised segmentation methods have broader applications and are more precise when provided with enough user input[42]. The semi-supervised is noted to be fast, but it performs worse than the supervised if the data assumptions fail to hold. However, recent approaches rather make assumptions that are pre-contained in the classifier[46].

6.2 Future directions

The future of abdominal organ segmentation is largely dependent on the availability of large and high quantity, and quality annotated datasets[25, 159]. Annotating medical images is extremely time-consuming and requires expert knowledge[139], which is costly hence the corresponding small medical image datasets. Currently, not too many annotated public datasets are available, and the ones available have become the basis for correlating the accuracy of distinct segmentation methods. On gallbladder, no open source CT images dataset of cholelithiasis and gallstones is available[94]. Supervised machine learning algorithm requires annotated data[13, 46], and supervised deep learning methods particularly requires a large labeled training set to achieve high accuracy[51] in their training[11]. On the other hand, the semi-supervised machine learning algorithm leverages on unannotated data[139] and may be necessary to be explored further by the research community to address the abdominal organ dataset limitations.

It can also be seen from the reviewed publications that majority of the datasets used are based on the CT modality, and very few of them are made up of the MRI and US modalities. The emerging MRI technology, with its high effectiveness in showing the difference between healthy and diseased soft tissues in the body[179], makes it the ideal modality for further and comprehensive analysis of the abdomen[167]. More than one imaging modality has been analyzed by physicians generally so as to assess better and evaluate the condition of abdominal organ(s)[30]. Hence, it would be necessary to advance research works on supervised and semi-supervised method(s) of segmenting abdominal organs using diverse

modalities simultaneously.

Finally, research interest on abdominal organs such as spleen, gallbladder, multi-organ, and pancreas has not gained much attention compared to the kidney and liver, and would be necessary to explore in both supervised and semi-supervised segmentation approaches.

7 Conclusions

In this paper, we have surveyed single and multi-abdominal organ(s) segmented based on supervised and semi-supervised methods, datasets, and abdominal organ segmentation evaluation metrics. Firstly, we discussed methods of supervised and semi-supervised segmentation. Then we presented supervised abdominal segmentation methods and their application on single and multi-organs. We also highlighted semi-supervised abdominal segmentation methods relative to single and multi-organs, and we assessed datasets in line with abdominal organ segmentation, while discussing abdominal organ segmentation over the stipulated period. Finally, we pointed out some future prospects relative to abdominal organ segmentation.

Abdominal organ(s) segmentation can be very efficient and effective when large and high quality annotated datasets are available. Also, the process of segmenting abdominal organ(s) is daunting due to issues with the technique of imaging and anatomy; the organ′s close proximity to adjacent organs, the similarity of texture and intensity of the adjacent organs, and the abdominal organ(s) shape′s low contrast and variability. However, the segmentation of abdominal organ(s) remains a critical area of research, and it is highly vital for computer-aided surgery, anatomical structure modeling, radiation therapy planning, tumor growth measurement, visualization prior to diagnosis, treatment, and surgical procedures, and computer-aided diagnosis which can save the life of patients.

Acknowledgements

This work was supported by National Natural Science Foundation of China (Nos. 61772242, 61976106 and 61572239), the China Postdoctoral Science Foundation (No. 2017M611737), the Six Talent Peaks Project in Jiangsu Province (No. DZXX-122), and the Key Special Project of Health and Family Planning Science and Technology in Zhenjiang City (No. SHW2017019). The authors would like to thank the Radiologists of the Medical Imaging Department of Affiliated Hospital of Jiangsu University.

References

[1] A. Reuben. Examination of the abdomen. *Clinical Liver Disease*, vol. 7, no. 6, pp. 143–150, 2016. DOI: 10.1002/cld.556.

[2] T. N. C. I. Dictionary, C. Terms, G. Nci, C. T. Widget. NCI dictionary of cancer terms. National Cancer Institute. [Online], Available: https://www.cancer.gov/publications/dictionaries/cancer-terms/def/abdominal, March 31, 2020.

[3] M. Bilal, V. Voin, N. Topale, J. Iwanaga, M. Loukas, R. S. Tubbs. The clinical anatomy of the physical examination of the abdomen: A comprehensive review. *Clinical Anatomy*, vol. 30, no. 3, pp. 352–356, 2017. DOI: 10.1002/ca.22832.

[4] R. Kaur, M. Juneja. Comparison of different renal imaging modalities: An overview. In *Progress in Intelligent Computing Techniques: Theory, Practice, and Applications*, P. K. Sa, M. N. Sahoo, M. Murugappan, Y. L. Wu, B. Majhi, Eds., Singapore: Springer, pp. 47–57, 2018. DOI: 10.1007/978-981-10-3373-5_4.

[5] M. Shojaee, A. Sabzghabaei, A. Heidari. Efficacy of new scoring system for diagnosis of abdominal injury after blunt abdominal trauma in patients referred to emergency department. *Chinese Journal of Traumatology*, vol. 23, no. 3, pp. 145–148, 2020. DOI: 10.1016/j.cjtee.2020.03.003.

[6] Z. J. Ricci, S. K. Oh, M. W. Stein, B. Kaul, M. Flusberg, V. Chernyak, A. M. Rozenblit, F. S. Mazzariol. Solid organ abdominal ischemia, part I: Clinical features, etiology, imaging findings, and management. *Clinical Imaging*, vol. 40, no. 4, pp. 720–731, 2016. DOI: 10.1016/j.clinimag.2016.02.014.

[7] Z. J. Ricci, F. S. Mazzariol, B. Kaul, S. K. Oh, V. Chernyak, M. Flusberg, M. W. Stein, A. M. Rozenblit. Hollow organ abdominal ischemia, part II: Clinical features, etiology, imaging findings and management. *Clinical Imaging*, vol. 40, no. 4, pp. 751–764, 2016. DOI: 10.1016/j.clinimag.2016.02.016.

[8] C. De Dios Soler-morejón, T. A. Lombardo-vaillant, T. O. Tamargo-Barbeito, M. L. N. G. Malbrain. Predicting abdominal surgery mortality: A model based on intra-abdominal pressure. *MEDICC Review*, vol. 19, no. 4, pp. 16–20, 2017. DOI: 10.37757/MR2017.V19.N4.5.

[9] P. Chinmayi, L. Agilandeeswari, M. Prabukumar. Survey of image processing techniques in medical image analysis: Challenges and methodologies. In *Proceedings of the 8th International Conference on Soft Computing and Pattern Recognition*, Springer, Vellore, India, pp. 460–471, 2016. DOI: 10.1007/978-3-319-60618-7_45.

[10] M. Dabass, S. Vashisth, R. Vig. Effectiveness of region growing based segmentation technique for various medical images – a study. In *Proceedings of the 4th International Conference on Recent Developments in Science, Engineering and Technology Data Science and Analytics*, Gurgaon, India, Springer, pp. 234–259, 2018. DOI: 10.1007/978-981-10-8527-7_21.

[11] C. Chen, C. Qin, H. Q. Qiu, G. Tarroni, J. M. Duan, W. J. Bai, D. Rueckert. Deep learning for cardiac image segmentation: A review. *Frontiers in Cardiovascular Medicine*, vol. 7, Article number 25, 2020. DOI: 10.3389/fcvm.2020.00025.

[12] G. Zhang, S. H. Dong, H. Xu, H. Y. Zhang, Y. J. Wu, Y. W. Zhang, X. M. Xi, Y. L. Yin. Correction learning for medical image segmentation. *IEEE Access*, vol. 7, pp. 143597–143607, 2019. DOI: 10.1109/ACCESS.2019.

2944849.

[13] S. A. Taghanaki, K. Abhishek, J. P. Cohen, J. Cohen-Adad, G. Hamarneh. Deep semantic segmentation of natural and medical images: A review. *Artificial Intelligence Review*, vol. 54, no. 1, pp. 137–178, 2021. DOI: 10.1007/s10462-020-09854-1.

[14] S. Ghosh, N. Das, I. Das, U. Maulik. Understanding deep learning techniques for image segmentation. *ACM Computing Surveys*, vol. 52, no. 4, Article number 73, 2019.

[15] X. M. Li, H. Chen, X. J. Qi, Q. Dou, C. W. Fu, P. A. Heng. H-DenseUNet: Hybrid densely connected UNet for liver and tumor segmentation from CT volumes. *IEEE Transactions on Medical Imaging*, vol. 37, no. 12, pp. 2663–2674, 2018. DOI: 10.1109/TMI.2018.2845918.

[16] Z. Z. Yang, L. Zhang, M. Zhang, J. Feng, Z. Wu, F. G. Ren, Y. Lv. Pancreas segmentation in abdominal CT scans using inter-/intra-slice contextual information with a cascade neural network. In *Proceedings of the 41st Annual International Conference of the IEEE Engineering in Medicine and Biology Society*, IEEE, Berlin, Germany, pp. 5937–5940, 2019. DOI: 10.1109/EMBC.2019.8856774.

[17] O. Gloger, R. Bülow, K. Tünnies, H. Völzke. Automatic gallbladder segmentation using combined 2D and 3D shape features to perform volumetric analysis in native and secretin – enhanced MRCP sequences. *Magnetic Resonance Materials in Physics, Biology and Medicine*, vol. 31, no. 3, pp. 383–397, 2018. DOI: 10.1007/s10334-017-0664-6.

[18] Y. K. Huo, J. Q. Liu, Z. B. Xu, R. L. Harrigan, A. Assad, R. G. Abramson, B. A. Landman. Robust multicontrast MRI spleen segmentation for splenomegaly using multi-atlas segmentation. *IEEE Transactions on Biomedical Engineering*, vol. 65, no. 2, pp. 336–343, 2018. DOI: 10.1109/TBME.2017.2764752.

[19] Y. Wang, Y. Y. Zhou, W. Shen, S. Park, E. K. Fishman, A. L. Yuille. Abdominal multi-organ segmentation with organ-attention networks and statistical fusion. *Medical Image Analysis*, vol. 55, pp. 88–102, 2019. DOI: 10.1016/j.media.2019.04.005.

[20] E. Gibson, F. Giganti, Y. P. Hu, E. Bonmati, S. Bandula, K. Gurusamy, B. Davidson, S. P. Pereira, M. J. Clarkson, D. C. Barratt. Automatic multi-organ segmentation on abdominal CT with dense V-Networks. *IEEE Transactions on Medical Imaging*, vol. 37, no. 8, pp. 1822–1834, 2018. DOI: 10.1109/TMI.2018.2806309.

[21] S. Q. Chen, X. Zhong, S. Dorn, N. Ravikumar, Q. H. Tao, X. L. Huang, M. Lell, M. Kachelriess, A. Maier. Improving generalization capability of multi-organ segmentation models using dual-energy CT. *IEEE Transactions on Radiation and Plasma Medical Sciences*, to be published. DOI: 10.1109/TRPMS.2021.3055199.

[22] K. L. Román, M. Inmaculada García Ocaña, N. L. Urzelai, M. Ángel González Ballester, I. M. Oliver. Medical image segmentation using deep learning. In *Deep Learning in Healthcare: Paradigms and Applications*, Springer, Cham, Germany, pp. 17–31, 2020. DOI: 10.1007/978-3-030-32606-7_2.

[23] S. S. Chouhan, A. Kaul, U. P. Singh. Image segmentation using computational intelligence techniques: Review. *Archives of Computational Methods in Engineering*, vol. 26, no. 3, pp. 533–596, 2019. DOI: 10.1007/s11831-018-9257-4.

[24] G. T. Wang, W. Q. Li, M. Aertsen, J. Deprest, S. Ourselin, T. Vercauteren. Aleatoric uncertainty estimation with test-time augmentation for medical image segmentation with convolutional neural networks. *Neurocomputing*, vol. 338, pp. 34–45, 2019. DOI: 10.1016/j.neucom.2019.01.103.

[25] H. Seo, M. B. Khuzani, V. Vasudevan, C. Huang, H. Y. Ren, R. X. Xiao, X. Jia, L. Xing. Machine learning techniques for biomedical image segmentation: An overview of technical aspects and introduction to state-of-art applications. *Medical Physics*, vol. 47, no. 5, pp. e148–e167, 2020.

[26] A. Chebli, A. Djebbar, H. F. Marouani. Semi-supervised learning for medical application: A survey. In *Proceedings of International Conference on Applied Smart Systems*, IEEE, Medea, Algeria, pp. 24–25, 2018. DOI: 10.1109/ICASS.2018.8651980.

[27] F. Kulwa, C. Li, X. Zhao, B. C. Cai, N. Xu, S. L. Qi, S. Chen, Y. Y. Teng. A state-of-the-art survey for microorganism image segmentation methods and future potential. *IEEE Access*, vol. 7, pp. 100243–100269, 2019. DOI: 10.1109/ACCESS.2019.2930111.

[28] I. Aganj, M. G. Harisinghani, R. Weissleder, B. Fischl. Unsupervised medical image segmentation based on the local center of mass. *Scientific Reports*, vol. 8, no. 1, Article number 13012, 2018. DOI: 10.1038/s41598-018-31333-5.

[29] M. Borga, T. Andersson, O. D. Leinhard. Semi-supervised learning of anatomical manifolds for atlas-based segmentation of medical images. In *Proceedings of the 23rd International Conference on Pattern Recognition*, IEEE, Cancun, Mexico, pp. 3146–3149, 2016. DOI: 10.1109/ICPR.2016.7900118.

[30] X. Yao, Y. Q. Song, Z. Liu. Advances on pancreas segmentation: A review. *Multimedia Tools and Applications*, vol. 79, pp. 6799–6821, 2019.

[31] H. R. Torres, S. Queirós, P. Morais, B. Oliveira, J. C. Fonseca, J. L. Vilaça. Kidney segmentation in ultrasound, magnetic resonance and computed tomography images: A systematic review. *Computer Methods and Programs in Biomedicine*, vol. 157, pp. 49–67, 2018. DOI: 10.1016/j.cmpb.2018.01.014.

[32] A. Gotra, L. Sivakumaran, G. Chartrand, K. N. Vu, F. Vandenbroucke-Menu, C. Kauffmann, S. Kadoury, B. Gallix, J. A. De Guise, A. Tang. Liver segmentation: Indications, techniques and future directions. *Insights into Imaging*, vol. 8, no. 4, pp. 377–392, 2017. DOI: 10.1007/s13244-017-0558-1.

[33] M. Moghbel, S. Mashohor, R. Mahmud, M. I. B. Saripan. Review of liver segmentation and computer assisted detection/diagnosis methods in computed tomography. *Artificial Intelligence Review*, vol. 50, no. 4, pp. 497–537, 2018. DOI: 10.1007/s10462-017-9550-x.

[34] H. Kumar, S. V. Desouza, M. S. Petrov. Automated pancreas segmentation from computed tomography and magnetic resonance images: A systematic review. *Computer Methods and Programs in Biomedicine*, vol. 178, pp. 319–328, 2019. DOI: 10.1016/j.cmpb.2019.07.002.

[35] R. M. Summers. Progress in fully automated abdominal CT interpretation. *American Journal of Roentgenology*, vol. 207, no. 1, pp. 67–79, 2016. DOI: 10.2214/AJR.15.15996.

[36] A. Rehman, F. G. Khan. A deep learning based review on abdominal images. *Multimedia Tools and Applications*, vol. 80, no. 20, pp. 30321–30352, 2021. DOI: 10.1007/S11042-020-09592-0.

[37] F. M. Meng, L. L. Guo, Q. B. Wu, H. L. Li. A new deep segmentation quality assessment network for refining bounding box based segmentation. *IEEE Access*, vol. 7, pp. 59514–59523, 2019. DOI: 10.1109/ACCESS.2019.2915121.

[38] Z. Jiang, C. Xu, X. H. Tu, T. Li, N. Gao. A Co-segmentation method for image pairs based on maximum common subgraph and GrabCut. In *Proceedings of the 2nd International Conference on Advances in Image Processing*, ACM, Chengdu, China, pp. 39–43, 2018. DOI: 10.1145/3239576.3239590.

[39] L. B. Yang, L. R. Mansaray, J. F. Huang, L. M. Wang. Optimal segmentation scale parameter, feature subset and classification algorithm for geographic object-based crop recognition using multisource satellite imagery. *Remote Sensing*, vol. 11, no. 5, Article number 514, 2019. DOI: 10.3390/rs11050514.

[40] A. Dosovitskiy, P. Fischer, J. T. Springenberg, M. Riedmiller, T. Brox. Discriminative unsupervised feature learning with exemplar convolutional neural networks. *IEEE Transactions on Pattern Analysis and Machine Intelligence*, vol. 38, no. 9, pp. 1734–1747, 2016. DOI: 10.1109/TPAMI.2015.2496141.

[41] S. Li, G. K. F. Tso, K. J. He. Bottleneck feature supervised U-Net for pixel-wise liver and tumor segmentation. *Expert Systems with Applications*, vol. 145, Article number 113131, 2020. DOI: 10.1016/j.eswa.2019.113131.

[42] Y. Deng, Y. Sun, Y. P. Zhu, Y. Xu, Q. X. Yang, S. Zhang, Z. Y. Wang, J. R. Sun, W. L. Zhao, X. B. Zhou, K. H. Yuan. A new framework to reduce doctor′s workload for medical image annotation. *IEEE Access*, vol. 7, pp. 107097–107104, 2019. DOI: 10.1109/ACCESS.2019.2917932.

[43] C. Y. Li, X. Y. Wang, S. Eberl, M. Fulham, Y. Yin, D. D. Feng. Supervised variational model with statistical inference and its application in medical image segmentation. *IEEE Transactions on Biomedical Engineering*, vol. 62, no. 1, pp. 196–207, 2015. DOI: 10.1109/TBME.2014.2344660.

[44] E. Kozegar, M. Soryani, H. Behnam, M. Salamati, T. Tan. Mass segmentation in automated 3-D breast ultrasound using adaptive region growing and supervised edge-based deformable model. *IEEE Transactions on Medical Imaging*, vol. 37, no. 4, pp. 918–928, 2018. DOI: 10.1109/TMI.2017.2787685.

[45] M. Xian, Y. T. Zhang, H. D. Cheng, F. Xu, B. Y. Zhang, J. Ding. R. Automatic breast ultrasound image segmentation: A survey. *Pattern Recognition*, vol. 79, pp. 340–355, 2018. DOI: 10.1016/j.patcog.2018.02.012.

[46] V. Cheplygina, M. de Bruijne, J. P. W. Pluim. Not-so-supervised: A survey of semi-supervised, multi-instance,and transfer learning in medical image analysis. *Medical Image Analysis*, vol. 54, pp. 280–296, 2019. DOI: 10.1016/j.media.2019.03.009.

[47] Z. Y. Shi, Y. X. Yang, T. M. Hospedales, T. Xiang. Weakly-supervised image annotation and segmentation with objects and attributes. *IEEE Transactions on Pattern Analysis and Machine Intelligence*, vol. 39, no. 12, pp. 2525–2538, 2017. DOI: 10.1109/TPAMI.2016.2645157.

[48] J. Enguehard, P. O'Halloran, A. Gholipour. Semi-supervised learning with deep embedded clustering for image classification and segmentation. *IEEE Access*, vol. 7, pp. 11093–11104, 2019. DOI: 10.1109/ACCESS.2019.2891970.

[49] Q. Chang, Z. N. Yan, Y. X. Lou, L. Axel, D. N. Metaxas. Soft-Label guided semi-supervised learning for Bi-ventricle segmentation in cardiac cine MRI. In *Proceedings of the 17th IEEE International Symposium on Biomedical Imaging*, IEEE, Iowa City, USA, pp. 1752–1755, 2020. DOI: 10.1109/ISBI45749.2020.9098546.

[50] B. Oliveira, S. Queirós, P. Morais, H. R. Torres, J. Gomes-Fonseca, J. C. Fonseca, J. L. Vilaça. A novel multi-atlas strategy with dense deformation field reconstruction for abdominal and thoracic multi-organ segmentation from computed tomography. *Medical Image Analysis*, vol. 45, pp. 108–120, 2018. DOI: 10.1016/j.media.2018.02.001.

[51] Y. Y. Zhou, Y. Wang, P. Tang, S. Bai, W. Shen, E. Fishman, A. Yuille. Semi-supervised 3D abdominal multi-organ segmentation via deep multi-planar Co-Training. In *Proceedings of IEEE Winter Conference on Applications of Computer Vision*, IEEE, Waikoloa, USA, pp. 121–140, 2019. DOI: 10.1109/WACV.2019.00020.

[52] T. W. Utomo, A. I. Cahyadi, I. Ardiyanto. Suction-based grasp point estimation in cluttered environment for robotic manipulator using deep learning-based affordance map. *International Journal of Automation and Computing*, vol. 18, no. 2, pp. 277–287, 2021. DOI: 10.1007/s11633-020-1260-1.

[53] J. H. Tao, J. Huang, Y. Li, Z. Lian, M. Y. Niu. Semi-supervised ladder networks for speech emotion recognition. *International Journal of Automation and Computing*, vol. 16, no. 4, pp. 437–448, 2019. DOI: 10.1007/s11633-019-1175-x.

[54] Z. H. Zhou. A brief introduction to weakly supervised learning. *National Science Review*, vol. 5, no. 1, pp. 44–53, 2018. DOI: 10.1093/nsr/nwx106.

[55] K. Y. Liu, X. B. Yang, H. L. Yu, J. S. Mi, P. X. Wang, X. J. Chen. Rough set based semi-supervised feature selection via ensemble selector. *Knowledge-based Systems*, vol. 165, pp. 282–296, 2019. DOI: 10.1016/j.knosys.2018.11.034.

[56] Y. W. Chong, Y. Ding, Q. Yan, S. M. Pan. Graph-based semi-supervised learning: A review. *Neurocomputing*, vol. 480, pp. 216–230, 2020.

[57] A. Zhao, G. Balakrishnan, F. Durand, J. V. Guttag, A. V. Dalca. Data augmentation using learned transformations for one-shot medical image segmentation. In *Proceedings of IEEE/CVF Conference on Computer Vision and Pattern Recognition*, IEEE, Long Beach, USA, pp. 8535–8545, 2019. DOI: 10.1109/CVPR.2019.00874.

[58] A. Meyer, S. Ghosh, D. Schindele, M. Schostak, S. Stober, C. Hansen, M. Rak. Uncertainty-aware temporal self-learning (UATS): Semi-supervised learning for segmentation of prostate zones and beyond. *Artificial Intelligence in Medicine*, vol. 116, Article number 102073, 2021. DOI: 10.1016/j.artmed.2021.102073.

[59] B. Gu, X. T. Yuan, S. C. Chen, H. Huang. New incremental learning algorithm for semi-supervised support vector machine. In *Proceedings of the 24th ACM SIGKDD International Conference on Knowledge Discovery & Data Mining*, ACM, London, UK, pp. 1475–1484, 2018. DOI: 10.1145/3219819.3220092.

[60] S. F. Ding, Z. B. Zhu, X. K. Zhang. An overview on semi-supervised support vector machine. *Neural Computing and Applications*, vol. 28, no. 5, pp. 969–978, 2017. DOI: 10.1007/s00521-015-2113-7.

[61] S. Yagasaki, N. Koizumi, Y. Nishiyama, R. Kondo, T. Imaizumi, N. Matsumoto, M. Ogawa, K. Numata. Estimating 3-dimensional liver motion using deep learning and 2-dimensional ultrasound images. *International Journal of Computer Assisted Radiology and Surgery*, vol. 15, no. 12, pp. 1989–1995, 2020. DOI: 10.1007/s11548-020-02265-1.

[62] P. H. Conze, V. Noblet, F. Rousseau, F. Heitz, R. Memeo, P. Pessaux. Random forests on hierarchical multi-scale supervoxels for liver tumor segmentation in dynamic contrast-enhanced CT scans. In *Proceedings of the 13th IEEE International Symposium on Biomedical Imaging*, IEEE, Prague, Czech Republic, pp. 416–419, 2016. DOI: 10.1109/ISBI.2016.7493296.

[63] M. Chung, J. Lee, M. Lee, J. Lee, Y. G. Shin. Deeply self-supervised contour embedded neural network applied to liver segmentation. *Computer Methods and Programs in Biomedicine*, vol. 192, Article number 105447, 2020. DOI: 10.1016/j.cmpb.2020.105447.

[64] M. F. Xu, Y. Wang, Y. Chi, X. S. Hua. Training liver vessel segmentation deep neural networks on noisy labels from contrast CT imaging. In *Proceedings of the 17th IEEE International Symposium on Biomedical Imaging*, IEEE, Iowa City, USA, pp. 1552–1555, 2020. DOI: 10.1109/ISBI45749.2020.9098509.

[65] R. M. Devi, V. Seenivasagam. Automatic segmentation and classification of liver tumor from CT image using feature difference and SVM based classifier-soft computing technique. *Soft Computing*, vol. 24, no. 24, pp. 18591–18598, 2020. DOI: 10.1007/s00500-020-05094-1.

[66] H. Seo, C. Huang, M. Bassenne, R. X. Xiao, L. Xing. Modified U-Net (mU-Net) with incorporation of object-dependent high level features for improved liver and liver-tumor segmentation in CT images. *IEEE Transactions on Medical Imaging*, vol. 39, no. 5, pp. 1316–1325, 2020. DOI: 10.1109/TMI.2019.2948320.

[67] X. Fang, S. Xu, B. J. Wood, P. K. Yan. Deep learning-based liver segmentation for fusion-guided intervention. *International Journal of Computer Assisted Radiology and Surgery*, vol. 15, no. 6, pp. 963–972, 2020. DOI: 10.1007/s11548-020-02147-6.

[68] X. K. Tang, E. Jafargholi Rangraz, W. Coudyzer, J. Bertels, D. Robben, G. Schramm, W. Deckers, G. Maleux, K. Baete, C. Verslype, M. J. Gooding, C. M. Deroose, J. Nuyts. Whole liver segmentation based on deep learning and manual adjustment for clinical use in SIRT. *European Journal of Nuclear Medicine and Molecular Imaging*, vol. 47, no. 12, pp. 2742–2752, 2020. DOI: 10.1007/s00259-020-04800-3.

[69] Y. S. Ng, Y. Xi, Y. X. Qian, L. Ananthakrishnan, T. C. Soesbe, M. Lewis, R. Lenkinski, J. R. Fielding. Use of spectral detector computed tomography to improve liver segmentation and volumetry. *Journal of Computer Assisted Tomography*, vol. 44, no. 2, pp. 197–203, 2020. DOI: 10.1097/RCT.0000000000000987.

[70] S. Almotairi, G. Kareem, M. Aouf, B. Almutairi, M. A. M. Salem. Liver tumor segmentation in CT scans using modified segnet. *Sensors*, vol. 20, no. 5, Article number 1516, 2020. DOI: 10.3390/s20051516.

[71] G. M. Cunha, K. A. Hasenstab, A. Higaki, K. Wang, T. Delgado, R. L. Brunsing, A. Schlein, A. Schwartzman, A. Hsiao, C. B. Sirlin, K. J. Fowler. Convolutional neural network-automated hepatobiliary phase adequacy evaluation may optimize examination time. *European Journal of Radiology*, vol. 124, Article number 108837, 2020. DOI: 10.1016/j.ejrad.2020.108837.

[72] A. A. Albishri, S. J. H. Shah, Y. Lee. CU-Net: Cascaded U-Net model for automated liver and lesion segmentation and summarization. In *Proceedings of IEEE International Conference on Bioinformatics and Biomedicine*, IEEE, San Diego, USA, pp. 1416–1423, 2019. DOI: 10.1109/BIBM47256.2019.8983266.

[73] Y. C. Wu, Q. Zhou, H. J. Hu, G. H. Rong, Y. W. Li, S. Y. Wang. Hepatic lesion segmentation by combining plain and contrast-enhanced CT images with modality weighted U-Net. In *Proceedings of IEEE International Conference on Image Processing*, IEEE, Taipei, China, pp. 255–259, 2019. DOI: 10.1109/ICIP.2019.8802942.

[74] I. Aganj, B. Fischl. Expected label value computation for atlas-based image segmentation. In *Proceedings of the 16th IEEE International Symposium on Biomedical Imaging*, IEEE, Venice, Italy, pp. 334–338, 2019. DOI: 10.1109/ISBI.2019.8759484.

[75] M. J. A. Jansen, H. J. Kuijf, J. P. W. Pluim. Optimal input configuration of dynamic contrast enhanced MRI in convolutional neural networks for liver segmentation. In *Proceedings of SPIE 10949, Medical Imaging 2019*, SPIE, San Diego, USA, Article number 109491V, 2019. DOI: 10.1117/12.2506770.

[76] T. Y. Su, W. T. Yang, T. C. Cheng, Y. F. He, C. J. Yang, Y. H. Fang. Computer-aided liver cirrhosis diagnosis via automatic liver segmentation and machine learning algorithm. In *Proceedings of SPIE 11050, International Forum on Medical Imaging in Asia 2019*, SPIE, Singapore, Article number 1105011, 2019. DOI: 10.1117/12.2521631.

[77] E. Dura, J. Domingo, E. Göçeri, L. Martí-Bonmatí. A method for liver segmentation in perfusion MR images using probabilistic atlases and viscous reconstruction. *Pattern Analysis and Applications*, vol. 21, no. 4, pp. 1083–1095, 2018. DOI: 10.1007/s10044-017-0666-z.

[78] W. Tang, D. S. Zou, S. Yang, J. Shi. DSL: Automatic liver segmentation with faster R-CNN and deeplab. In *Proceedings of the 27th International Conference on Artifi-*

cial Neural Networks and Machine Learning, Springer, Rhodes, Greece, pp. 137–147, 2018. DOI: 10.1007/978-3-030-01421-6_14.

[79] Q. Dou, L. Q. Yu, H. Chen, Y. M. Jin, X. Yang, J. Qin, P. A. Heng. 3D deeply supervised network for automated segmentation of volumetric medical images. *Medical Image Analysis*, vol. 41, pp. 40–54, 2017. DOI: 10.1016/j.media.2017.05.001.

[80] A. Ben-Cohen, I. Diamant, E. Klang, M. Amitai, H. Greenspan. Fully convolutional network for liver segmentation and lesions detection. In *Proceedings of the 1st International Workshop on Deep Learning and Data Labeling for Medical Applications*, Springer, Athens, Greece, pp. 77–85, 2016. DOI: 10.1007/978-3-319-46976-8_9.

[81] B. C. Anil, P. Dayananda. Automatic liver tumor segmentation based on multi-level deep convolutional networks and fractal residual network. *IETE Journal of Research*, to be published. DOI: 10.1080/03772063.2021.1878066.

[82] N. Alalwan, A. Abozeid, A. A. ElHabshy, A. Alzahrani. Efficient 3D deep learning model for medical image semantic segmentation. *Alexandria Engineering Journal*, vol. 60, no. 1, pp. 1231–1239, 2021. DOI: 10.1016/j.aej.2020.10.046.

[83] L. B. da Cruz, J. D. L. Araújo, J. L. Ferreira, J. O. B. Diniz, A. C. Silva, J. D. S. De Almeida, A. C. De Paiva, M. Gattass. Kidney segmentation from computed tomography images using deep neural network. *Computers in Biology and Medicine*, vol. 123, pp. 103906, 2020. DOI: 10.1016/J.COMPBIOMED.2020.103906.

[84] C. Jin, F. Shi, D. H. Xiang, X. Q. Jiang, B. Zhang, X. M. Wang, W. F. Zhu, E. T. Gao, X. J. Chen. 3D fast automatic segmentation of kidney based on modified AAM and random forest. *IEEE Transactions on Medical Imaging*, vol. 35, no. 6, pp. 1395–1407, 2016. DOI: 10.1109/TMI.2015.2512606.

[85] T. Pan, G. Y. Yang, C. X. Wang, Z. W. Lu, Z. W. Zhou, Y. Y. Kong, L. J. Tang, X. M. Zhu, J. L. Dillenseger, H. Z. Shu, J. L. Coatrieux. A Multi-task convolutional neural network for renal tumor segmentation and classification using multi-phasic CT images. In *Proceedings of IEEE International Conference on Image Processing*, IEEE, Taipei, China, pp. 80–813, 2019. DOI: 10.1109/ICIP.2019.8802924.

[86] Z. Fatemeh, S. Nicola, K. Satheesh, U. Eranga. Ensemble U-net-based method for fully automated detection and segmentation of renal masses on computed tomography images. *Medical Physics*, vol. 47, no. 9, pp. 4032–4044, 2020. DOI: 10.1002/mp.14193.

[87] S. Yin, Q. M. Peng, H. M. Li, Z. Q. Zhang, X. G. You, K. Fischer, S. L. Furth, G. E. Tasian, Y. Fan. Automatic kidney segmentation in ultrasound images using subsequent boundary distance regression and pixelwise classification networks. *Medical Image Analysis*, vol. 60, Article number 101602, 2020. DOI: 10.1016/j.media.2019.101602.

[88] J. Park, S. Bae, S. Seo, S. Park, J. I. Bang, J. H. Han, W. W. Lee, J. S. Lee. Measurement of glomerular filtration rate using quantitative SPECT/CT and deep-learning-based kidney segmentation. *Scientific Reports*, vol. 9, no. 1, Article number 4223, 2019. DOI: 10.1038/s41598-019-40710-7.

[89] H. Abdeltawab, M. Shehatal, A. Shalaby, S. Mesbah, M. El-Baz, M. Ghazal, Y. Alkhali, M. Abouel-Ghar, A. C. Dwyer, M. El-Melegy, A. El-Baz. A new 3D CNN-based CAD system for early detection of acute renal transplant rejection. In *Proceedings of the 24th International Conference on Pattern Recognition*, IEEE, Beijing, China, pp. 3898–3903, 2018. DOI: 10.1109/ICPR.2018.8545713.

[90] M. Haghighi, S. K. Warfield, S. Kurugol. Automatic renal segmentation in DCE-MRI using convolutional neural networks. In *Proceedings of the 15th IEEE International Symposium on Biomedical Imaging*, IEEE, Washington DC,USA, pp. 1534–1537, 2018. DOI:10.1109/ISBI.2018.8363865.

[91] H. Ravishankar, S. Thiruvenkadam, R. Venkataramani, V. Vaidya. Joint deep learning of foreground, background and shape for robust contextual segmentation. In *Proceedings of the 25th International Conference on Information Processing in Medical Imaging*, Springer, Boone, USA, pp. 622–632, 2017. DOI: 10.1007/978-3-319-59050-9_49.

[92] P. R. Tabrizi, A. Mansoor, J. J. Cerrolaza, J. Jago, M. G. Linguraru. Automatic kidney segmentation in 3D pediatric ultrasound images using deep neural networks and weighted fuzzy active shape model. In *Proceedings of the 15th IEEE International Symposium on Biomedical Imaging*, IEEE, Washington, USA, pp. 1170–1173, 2018. DOI: 10.1109/ISBI.2018.8363779.

[93] F. Khalifa, A. Soliman, A. C. Dwyer, G. Gimel'Farb, A. El-Baz. A random forest-based framework for 3D kidney segmentation from dynamic contrast-enhanced CT images. In *Proceedings of IEEE International Conference on Image Processing*, IEEE, Phoenix, USA, pp. 3399–3403, 2016. DOI: 10.1109/ICIP.2016.7532990.

[94] S. C. Pang, T. Ding, S. B. Qiao, F. Meng, S. Wang, P. B. Li, X. Wang. A novel YOLOv3-arch model for identifying cholelithiasis and classifying gallstones on CT images. *PLoS One*, vol. 14, no. 6, Article number e0217647, 2019. DOI: 10.1371/journal.pone.0217647.

[95] J. Zhang, L. R. Zhu, L. W. Yao, X. W. Ding, D. Chen, H. L. Wu, Z. H. Lu, W. Zhou, L. H. Zhang, P. An, B. Xu, W. Tan, S. Hu, F. Cheng, H. G. Yu. Deep learning-based pancreas segmentation and station recognition system in EUS: Development and validation of a useful training tool (with video). *Gastrointestinal Endoscopy*, vol. 92, no. 4, pp. 874–885, 2020. DOI: 10.1016/j.gie.2020.04.071.

[96] M. Nishio, S. Noguchi, K. Fujimoto. Automatic pancreas segmentation using coarse-scaled 2D model of deep learning: Usefulness of data augmentation and deep U-net. *Applied Sciences*, vol. 10, no. 10, Article number 3360, 2020. DOI: 10.3390/app10103360.

[97] H. Y. Zheng, Y. F. Chen, X. D. Yue, C. Ma, X. H. Liu, P. P. Yang, J. P. Lu. Deep pancreas segmentation with uncertain regions of shadowed sets. *Magnetic Resonance Imaging*, vol. 68, pp. 45–52, 2020. DOI: 10.1016/j.mri.2020.01.008.

[98] F. Y. Li, W. S. Li, Y. C. Shu, S. Qin, B. Xiao, Z. W. Zhan.

Multiscale receptive field based on residual network for pancreas segmentation in CT images. *Biomedical Signal Processing and Control*, vol. 57, Article number 101828, 2020. DOI: 10.1016/j.bspc.2019.101828.

[99] Y. Zhang, J. Wu, S. M. Wang, Y. L. Liu, Y. F. Chen, E. X. Wu, X. Y. Tang. Liver guided pancreas segmentation. In *Proceedings of the IEEE 17th International Symposium on Biomedical Imaging*, IEEE, Iowa City, USA, pp. 1201–1204, 2020. DOI: 10.1109/ISBI45749.2020.9098388.

[100] W. H. Yu, H. Chen, L. S. Wang. Dense attentional network for pancreas segmentation in abdominal CT scans. In *Proceedings of the 2nd International Conference on Artificial Intelligence and Pattern Recognition*, ACM, Beijing, China, pp. 83–87, 2019. DOI: 10.1145/3357254.3357259.

[101] W. Z. Wang, Q. Y. Song, R. W. Feng, T. T. Chen, J. T. Chen, D. Z. Chen, J. Wu. A fully 3D cascaded framework for pancreas segmentation. In *Proceedings of the 17th IEEE International Symposium on Biomedical Imaging*, IEEE, Iowa City, USA, pp. 207–211, 2020. DOI: 10.1109/ISBI45749.2020.9098473.

[102] Y. Z. Man, Y. S. B. Huang, J. Y. Feng, X. Li, F. Wu. Deep Q learning driven CT pancreas segmentation with geometry-aware U-Net. *IEEE Transactions on Medical Imaging*, vol. 38, no. 8, pp. 1971–1980, 2019. DOI: 10.1109/TMI.2019.2911588.

[103] A. Farag, L. Lu, H. R. Roth, J. M. Liu, E. Turkbey, R. M. Summers. A bottom-up approach for pancreas segmentation using cascaded superpixels and (deep) image patch labeling. *IEEE Transactions on Image Processing*, vol. 26, no. 1, pp. 386–399, 2017. DOI: 10.1109/TIP.2016.2624198.

[104] N. N. Zhao, N. Tong, D. Ruan, K. Sheng. Fully automated pancreas segmentation with two-stage 3D convolutional neural networks. In *Proceedings of the 22nd International Conference on Medical Image Computing and Computer Assisted Intervention*, Springer, Shenzhen, China, pp. 201–209, 2019. DOI: 10.1007/978-3-030-32245-8_23.

[105] M. P. Heinrich, M. Blendowski, O. Oktay. TernaryNet: Faster deep model inference without GPUs for medical 3D segmentation using sparse and binary convolutions. *International Journal of Computer Assisted Radiology and Surgery*, vol. 13, no. 9, pp. 1311–1320, 2018. DOI: 10.1007/s11548-018-1797-4.

[106] H. Moon, Y. K. Huo, R. G. Abramson, R. A. Peters, A. Assad, T. K. Moyo, M. R. Savona, B. A. Landman. Acceleration of spleen segmentation with end-to-end deep learning method and automated pipeline. *Computers in Biology and Medicine*, vol. 107, pp. 109–117, 2019. DOI: 10.1016/j.compbiomed.2019.01.018.

[107] H. Wang, G. T. Wang, Z. H. Xu, W. H. Lei, S. T. Zhang. High- and low-level feature enhancement for medical image segmentation. In *Proceedings of the 10th International Workshop on Machine Learning in Medical Imaging*, Springer, Shenzhen, China, pp. 611–619, 2019. DOI: 10.1007/978-3-030-32692-0_70.

[108] J. Q. Liu, Y. K. Huo, Z. B. Xu, A. Assad, R. G. Abramson, B. A. Landman. Multi-atlas spleen segmentation on CT using adaptive context learning. In *Proceedings of SPIE 10133, Medical Imaging 2017*, SPIE, Orlando, USA, Article number 1013309, 2017. DOI: 10.1117/12.2254437.

[109] L. Zhang, J. M. Zhang, P. Y. Shen, G. M. Zhu, P. Li, X. Y. Lu, H. Zhang, S. A. Shah, M. Bennamoun. Block level skip connections across cascaded V-Net for multi-organ segmentation. *IEEE Transactions on Medical Imaging*, vol. 39, no. 9, pp. 2782–2793, 2020. DOI: 10.1109/TMI.2020.2975347.

[110] S. Park, L. C. Chu, E. K. Fishman, A. L. Yuille, B. Vogelstein, K. W. Kinzler, K. M. Horton, R. H. Hruban, E. S. Zinreich, D. Fadaei Fouladi, S. Shayesteh, J. Graves, S. Kawamoto. Annotated normal CT data of the abdomen for deep learning: Challenges and strategies for implementation. *Diagnostic and Interventional Imaging*, vol. 101, no. 1, pp. 35–44, 2020. DOI: 10.1016/j.diii.2019.05.008.

[111] Y. H. Chen, D. Ruan, J. Y. Xiao, L. X. Wang, B. Sun, R. Saouaf, W. S. Yang, D. B. Li, Z. Y. Fan. Fully automated multiorgan segmentation in abdominal magnetic resonance imaging with deep neural networks. *Medical Physics*, vol. 47, no. 10, pp. 4971–4982, 2020. DOI: 10.1002/mp.14429.

[112] X. Fang, P. K. Yan. Multi-organ segmentation over partially labeled datasets with multi-scale feature abstraction. *IEEE Transactions on Medical Imaging*, vol. 39, no. 11, pp. 3619–3629, 2020. DOI: 10.1109/TMI.2020.3001036.

[113] Y. Ahn, J. S. Yoon, S. S. Lee, H. I. Suk, J. H. Son, Y. S. Sung, Y. Lee, B. K. Kang, H. S. Kim. Deep learning algorithm for automated segmentation and volume measurement of the liver and spleen using portal venous phase computed tomography images. *Korean Journal of Radiology*, vol. 21, no. 8, pp. 987–997, 2020. DOI: 10.3348/kjr.2020.0237.

[114] M. P. Heinrich, O. Oktay, N. Bouteldja. OBELISK-Net: Fewer layers to solve 3D multi-organ segmentation with sparse deformable convolutions. *Medical Image Analysis*, vol. 54, pp. 1–9, 2019. DOI: 10.1016/j.media.2019.02.006.

[115] H. Kakeya, T. Okada, Y. Oshiro. 3D U-JAPA-Net: Mixture of convolutional networks for abdominal multi-organ CT segmentation. In *Proceedings of the 21st International Conference on Medical Image Computing and Computer Assisted Intervention*, Springer, Granada, Spain, pp. 352–360, 2018. DOI: 10.1007/978-3-030-00937-3_49.

[116] R. G. Bisen, A. M. Rajrkar, R. R. Manthalkar. Segmentation, detection, and classification of liver tumors for designing a CAD system. In *Proceedings of Conference on Computing in Engineering and Technology*, Springer, Singapore, pp. 103–111, 2019. DOI: 10.1007/978-981-32-9515-5_10.

[117] Y. X. Chen, S. Y. Li, S. Yang, W. Y. Luo. *Liver Segmentation in CT Images with Adversarial Learning*. In *Proceedings of the 15th International Conference on Intelligent Computing Theories and Application*, Springer, Nanchang, China, pp. 470–480, 2019. DOI: 10.1007/978-3-030-26763-6_45.

[118] S. K. Asrani, H. Devarbhavi, J. Eaton, P. S. Kamath.

Burden of liver diseases in the world. *Journal of Hepatology*, vol. 70, no. 1, pp. 151–171, 2019. DOI: 10.1016/j.jhep.2018.09.014.

[119] Z. Liu, Y. Q. Song, V. S. Sheng, L. M. Wang, R. Jiang, X. L. Zhang, D. Q. Yuan. Liver CT sequence segmentation based with improved U-Net and graph cut. *Expert Systems with Applications*, vol. 126, pp. 54–63, 2019. DOI: 10.1016/j.eswa.2019.01.055.

[120] Y. Zhang, J. Wu, B. X. Jiang, D. C. Ji, Y. F. Chen, E. X. Wu, X. Y. Tang. Deep learning and unsupervised fuzzy C-means based level-set segmentation for liver tumor. In *Proceedings of the 17th IEEE International Symposium on Biomedical Imaging*, IEEE, Iowa City, USA, pp. 1193–1196, 2020. DOI: 10.1109/ISBI45749.2020.9098701.

[121] R. Dey, Y. Hong. Hybrid cascaded neural network for liver lesion segmentation. In *Proceedings of the 17th IEEE International Symposium on Biomedical Imaging*, IEEE, Iowa City, USA, pp. 1173–1177, 2020. DOI: 10.1109/ISBI45749.2020.9098656.

[122] Z. Farooq, A. H. Behzadi, J. D. Blumenfeld, Y. Z. Zhao, M. R. Prince. Comparison of MRI segmentation techniques for measuring liver cyst volumes in autosomal dominant polycystic kidney disease. *Clinical Imaging*, vol. 47, pp. 41–46, 2018. DOI: 10.1016/j.clinimag.2017.07.004.

[123] X. S. Hou, C. M. Xie, F. Y. Li, J. P. Wang, C. F. Lv, G. T. Xie, Y. Nan. A triple-stage self-guided network for kidney tumor segmentation. In *Proceedings of the 17th IEEE International Symposium on Biomedical Imaging*, IEEE, Iowa City, USA, pp. 341–344, 2020. DOI: 10.1109/ISBI45749.2020.9098609.

[124] M. Tubay, S. Zelasko. Multimodality imaging of the gallbladder: Spectrum of pathology and associated imaging findings. *Current Radiology Reports*, vol. 4, no. 5, Article number 21, 2016. DOI: 10.1007/s40134-016-0148-x.

[125] V. Muneeswaran, M. P. Rajasekaran. Automatic segmentation of gallbladder using bio-inspired algorithm based on a spider web construction model. *The Journal of Supercomputing*, vol. 75, no. 6, pp. 3158–3183, 2019. DOI: 10.1007/s11227-017-2230-4.

[126] C. Serra, F. Pallotti, M. Bortolotti, C. Caputo, C. Felicani, R. D. Giorgio, G. Barbara, E. Nardi, A. M. M. Labate. A new reliable method for evaluating gallbladder dynamics: The 3-dimensional sonographic examination. *Journal of Ultrasound in Medicine*, vol. 35, no. 2, pp. 297–304, 2016. DOI: 10.7863/ultra.14.10033.

[127] G. V. Timokhov, E. A. Semenova. The decision support algorithm for a surgeon in preoperative planning of minilaparotomy gallbladder surgery from an arbitrary incision site. In *Proceedings of Ural Symposium on Biomedical Engineering, Radioelectronics and Information Technology*, IEEE, Yekaterinburg, Russia, pp. 74–77, 2019. DOI: 10.1109/USBEREIT.2019.8736587.

[128] S. Tognarelli, M. Brancadoro, V. Dolosor, A. Menciassi. Soft tool for gallbladder retraction in minimally invasive surgery based on layer jamming. In *Proceedings of the 7th IEEE International Conference on Biomedical Robotics and Biomechatronics*, IEEE, Enschede, Netherlands, pp. 67–72, 2018. DOI: 10.1109/BIOROB.2018.8488152.

[129] L. L. Cong, Z. Q. Cai, P. Guo, C. Chen, D. C. Liu, W. Z. Li, L. Wang, Y. L. Zhao, S. B. Si, Z. M. Geng. Decision of surgical approach for advanced gallbladder adenocarcinoma based on a Bayesian network. *Journal of Surgical Oncology*, vol. 116, no. 8, pp. 1123–1131, 2017. DOI: 10.1002/jso.24797.

[130] Z. Zhang, N. Li, H. Y. Gao, Z. Q. Cai, S. B. Si, Z. M. Geng. Preoperative analysis for clinical features of unsuspected gallbladder cancer based on random forest. In *Proceedings of IEEE International Conference on Industrial Engineering and Engineering Management*, IEEE, Bangkok, Thailand, pp. 1160–1164, 2018. DOI: 10.1109/IEEM.2018.8607352.

[131] A. P. Wasnik, M. S. Davenport, R. K. Kaza, W. J. Weadock, A. Udager, N. Keshavarzi, B. Nan, K. E. Maturen. Diagnostic accuracy of MDCT in differentiating gallbladder cancer from acute and xanthogranulomatous cholecystitis. *Clinical Imaging*, vol. 50, pp. 223–228, 2018. DOI: 10.1016/j.clinimag.2018.04.010.

[132] B. J. Ha, S. Park. Classification of gallstones using Fourier-transform infrared spectroscopy and photography. *Biomaterials Research*, vol. 22, no. 1, Article number 18, 2018. DOI: 10.1186/s40824-018-0128-8.

[133] S. Liu, Q. Liu, X. R. Yuan, R. Y. Hu, S. J. Liang, S. H. Feng, Y. H. Ai, Y. Zhang. Automatic pancreas segmentation via coarse location and ensemble learning. *IEEE Access*, vol. 8, pp. 2906–2914, 2020. DOI: 10.1109/ACCESS.2019.2961125.

[134] P. J. Hu, X. Li, Y. Tian, T. Y. Tang, T. S. Zhou, X. L. Bai, S. Q. Zhu, T. B. Liang, J. S. Li. Automatic pancreas segmentation in CT images with distance-based saliency-aware DenseASPP network. *IEEE Journal of Biomedical and Health Informatics*, vol. 25, no. 5, pp. 1601–1611, 2021. DOI: 10.1109/JBHI.2020.3023462.

[135] I. Gutenko, K. Dmitriev, A. E. Kaufman, M. A. Barish. AnaFe: Visual analytics of image-derived temporal features - focusing on the spleen. *IEEE Transactions on Visualization and Computer Graphics*, vol. 23, no. 1, pp. 171–180, 2017. DOI: 10.1109/TVCG.2016.2598463.

[136] Y. K. Huo, Z. B. Xu, S. X. Bao, C. Bermudez, H. Moon, P. Parvathaneni, T. K. Moyo, M. R. Savona, A. Assad, R. G. Abramson, B. A. Landman. Splenomegaly segmentation on multi-modal MRI using deep convolutional networks. *IEEE Transactions on Medical Imaging*, vol. 38, no. 5, pp. 1185–1196, 2019. DOI: 10.1109/TMI.2018.2881110.

[137] A. Wood, S. M. R. Soroushmehr, N. Farzaneh, D. Fessell, K. R. Ward, J. Gryak, D. Kahrobaei, K. Na. Fully automated spleen localization and segmentation using machine learning and 3D active contours. In *Proceedings of the 40th Annual International Conference of the IEEE Engineering in Medicine and Biology Society*, IEEE, Honolulu, USA, pp. 53–56, 2018. DOI: 10.1109/EMBC.2018.8512182.

[138] T. Küstner, S. Müller, M. Fischer, J. Weiss, K. Nikolaou, F. Bamberg, B. Yang, F. Schick, S. Gatidis. Semantic organ segmentation in 3D whole-body MR images. In *Proceedings of the 25th IEEE International Conference on Image Processing*, IEEE, Athens, Greece, pp. 3498–3502, 2018. DOI: 10.1109/ICIP.2018.8451205.

[139] H. Zheng, L. F. Lin, H. J. Hu, Q. W. Zhang, Q. Q. Chen, Y. Iwamoto, X. H. Han, Y. W. Chen, R. F. Tong, J. Wu. Semi-supervised segmentation of liver using adversarial learning with deep atlas prior. In *Proceedings of the 22nd International Conference on Medical Image Computing and Computer Assisted Intervention*, Springer, Shenzhen, China, pp. 148–156, 2019. DOI: 10.1007/978-3-030-32226-7_17.

[140] F. Lu, F. Wu, P. J. Hu, Z. Peng, D. X. Kong. Automatic 3D liver location and segmentation via convolutional neural network and graph cut. *International Journal of Computer Assisted Radiology and Surgery*, vol. 12, no. 2, pp. 171–182, 2017. DOI: 10.1007/s11548-016-1467-3.

[141] S. Sangewar, P. Daigavane, G. Somulu. A comparative study of k-means and graph cut method of liver segmentation. In *Proceedings of the 3rd International Conference on Electrical, Computer, Electronics & Biomedical Engineering & 3rd International Conference on Business, Economics, and Environment Issues*, Bangkok, Thailand, pp. 2540–2543, 2017.

[142] W. W. Wu, Z. H. Zhou, S. C. Wu, Y. H. Zhang. Automatic liver segmentation on volumetric CT images using supervoxel-based graph cuts. *Computational and Mathematical Methods in Medicine*, vol. 2016, Article number 9093721, 2016.

[143] M. Liao, Y. Q. Zhao, X. Y. Liu, Y. Z. Zeng, B. J. Zou, X. F. Wang, F. Y. Shih. Automatic liver segmentation from abdominal CT volumes using graph cuts and border marching. *Computer Methods and Programs in Biomedicine*, vol. 143, pp. 1–12, 2017. DOI: 10.1016/j.cmpb.2017.02.015.

[144] Q. Huang, H. Ding, X. D. Wang, G. Z. Wang. Fully automatic liver segmentation in CT images using modified graph cuts and feature detection. *Computers in Biology and Medicine*, vol. 95, pp. 198–208, 2018. DOI: 10.1016/j.compbiomed.2018.02.012.

[145] C. L. Wang, H. R. Roth, T. Kitasaka, M. Oda, Y. Hayashi, Y. Yoshino, T. Yamamoto, N. Sassa, M. Goto, K. Mori. Precise estimation of renal vascular dominant regions using spatially aware fully convolutional networks, tensor-cut and Voronoi diagrams. *Computerized Medical Imaging and Graphics*, vol. 77, Article number 101642, 2019. DOI: 10.1016/j.compmedimag.2019.101642.

[146] U. Yoruk, B. A. Hargreaves, S. S. Vasanawala. Automatic renal segmentation for MR urography using 3D-GrabCut and random forests. *Magnetic Resonance in Medicine*, vol. 79, no. 3, pp. 1696–1707, 2018. DOI: 10.1002/mrm.26806.

[147] Q. Zheng, S. Warner, G. Tasian, Y. Fan. A dynamic graph cuts method with integrated multiple feature maps for segmenting kidneys in 2D ultrasound images. *Academic Radiology*, vol. 25, no. 9, pp. 1136–1145, 2018. DOI: 10.1016/j.acra.2018.01.004.

[148] Y. D. Xia, D. Yang, Z. D. Yu, F. Z. Liu, J. Z. Cai, L. Q. Yu, Z. T. Zhu, D. G. Xu, A. Yuille, H. Roth. Uncertainty-aware multi-view co-training for semi-supervised medical image segmentation and domain adaptation. *Medical Image Analysis*, vol. 65, pp. 101766, 2020. DOI: 10.1016/j.media.2020.101766.

[149] K. Chaitanya, N. Karani, C. F. Baumgartner, E. Erdil, A. Becker, O. Donati, E. Konukoglu. Semi-supervised task-driven data augmentation for medical image segmentation. *Medical Image Analysis*, vol. 68, pp. 101934, 2021. DOI: 10.1016/j.media.2020.101934.

[150] Y. D. Xia, F. Z. Liu, D. Yang, J. Z. Cai, L. Q. Yu, Z. T. Zhu, D. G. Xu, A. Yuille, H. Roth. 3D semi-supervised learning with uncertainty-aware multi-view Co-training. In *Proceedings of IEEE Winter Conference on Applications of Computer Vision*, IEEE, Snowmass, USA, pp. 3635–3644, 2020. DOI: 10.1109/WACV45572.2020.9093608.

[151] R. D. Soberanis-Mukul, N. Navab, S. Albarqouni. Uncertainty-based graph convolutional networks for organ segmentation refinement. In *Proceedings of International Conference on Medical Imaging with Deep Learning*, Montréal, Canada, pp. 755–769, 2020.

[152] Y. C. Tang, Y. K. Huo, Y. X. Xiong, H. Moon, A. Assad, T. K. Moyo, M. R. Savona, R. Abramson, B. A. Landman. Improving splenomegaly segmentation by learning from heterogeneous multi-source labels. In *Proceedings of SPIE 10949, Medical Imaging 2019: Image Processing*, SPIE, San Diego, USA, Article number 1094908, 2019. DOI: 10.1117/12.2512842.

[153] R. Huang, Y. J. Zheng, Z. Q. Hu, S. T. Zhang, H. S. Li. Multi-organ segmentation via Co-training weight-averaged models from few-organ datasets. In *Proceedings of the 23rd International Conference on Medical Image Computing and Computer Assisted Intervention*, Springer, Lima, Peru, pp. 146–155, 2020. DOI: 10.1007/978-3-030-59719-1_15.

[154] T. Takaoka, Y. Mochizuki, H. Ishikawa. Multiple-organ segmentation by graph cuts with supervoxel nodes. In *Proceedings of the 15th IAPR International Conference on Machine Vision Applications*, IEEE, Nagoya, Japan, pp. 424–427, 2017. DOI: 10.23919/MVA.2017.7986891.

[155] R. Kéchichian, S. Valette, M. Desvignes. Automatic multiorgan segmentation via multiscale registration and graph cut. *IEEE Transactions on Medical Imaging*, vol. 37,no. 12,pp. 2739–2749,2018.DOI:10.1109/TMI.2018.2851780.

[156] A. Saito, S. Nawano, A. Shimizu. Fast approximation for joint optimization of segmentation, shape, and location priors, and its application in gallbladder segmentation. *International Journal of Computer Assisted Radiology and Surgery*, vol. 12, no. 5, pp. 743–756, 2017. DOI: 10.1007/s11548-017-1571-z.

[157] Y. K. Huo, J. Q. Liu, Z. B. Xu, R. L. Harrigan, A. Assad, R. G. Abramson, B. A. Landman. Multi-atlas segmentation enables robust multi-contrast MRI spleen segmentation for splenomegaly. In *Proceedings of SPIE 10133, Medical Imaging 2017: Image Processing*, SPIE, Orlando, USA, Article number 101330A, 2017. DOI: 10.1117/12.2254147.

[158] H. Müller, D. Unay. Retrieval from and understanding of large-scale multi-modal medical datasets: A review. *Transactions on Multimedia*, vol. 19, no. 9, pp. 2093–2104, 2017. DOI: 10.1109/TMM.2017.2729400.

[159] N. Tajbakhsh, L. Jeyaseelan, Q. Li, J. N. Chiang, Z. H. Wu, X. W. Ding. Embracing imperfect datasets: A review of deep learning solutions for medical image seg-

mentation. *Medical Image Analysis*, vol. 63, no. 101693, 2020.

[160] Z. Q. Cai, P. Guo, S. Li, L. L. Cong, Z. M. Geng. Gallbladder diagnosis and importance analysis based on bayesian network. In *Proceedings of the 23rd International Conference on Industrial Engineering and Engineering Management 2016: Theory and Application of Industrial Engineering*, pp. 269–273, 2017. DOI: 10.2991/978-94-6239-255-7_48.

[161] N. Jain, V. Kumar. Liver ultrasound image segmentation using region-difference filters. *Journal of Digital Imaging*, vol. 30, no. 3, pp. 376–390, 2017. DOI: 10.1007/s10278-016-9934-5.

[162] C. F. Shi, Y. Z. Cheng, F. Liu, Y. D. Wang, J. Bai, S. Tamura. A hierarchical local region-based sparse shape composition for liver segmentation in CT scans. *Pattern Recognition*, vol. 50, pp. 88–106, 2016. DOI: 10.1016/j.patcog.2015.09.001.

[163] M. Liao, Y. Q. Zhao, W. Wang, Y. Z. Zeng, Q. Yang, F. Y. Shih, B. J. Zou. Efficient liver segmentation in CT images based on graph cuts and bottleneck detection. *Physica Medica*, vol. 32, no. 11, pp. 1383–1396, 2016. DOI: 10.1016/j.ejmp.2016.10.002.

[164] M. A. Azam, K. B. Khan, M. Aqeel, A. R. Chishti, M. N. Abbasi. Analysis of the MIDAS and OASIS biomedical databases for the application of multimodal image processing. In *Proceedings of the 2nd International Conference on Intelligent Technologies and Applications*, Springer, Bahawalpur, Pakistan, pp. 581–592, 2020. DOI: 10.1007/978-981-15-5232-8_50.

[165] A. Qayyum, A. Lalande, F. Meriaudeau. Automatic segmentation of tumors and affected organs in the abdomen using a 3D hybrid model for computed tomography imaging. *Computers in Biology and Medicine*, vol. 127, Article number 104097, 2020. DOI: 10.1016/j.compbiomed.2020.104097.

[166] A. L. Simpson, M. Antonelli, S. Bakas, M. Bilello, K. Farahani, B. van Ginneken, A. Kopp-Schneider, B. A. Landman, G. Litjens, B. Menze, O. Ronneberger, R. M. Summers, P. Bilic, P. F. Christ, R. K. G. Do, M. Gollub, J. Golia-Pernicka, S. H. Heckers, W. R. Jarnagin, M. K. McHugo, S. Napel, E. Vorontsov, L. Maier-Hein, M. J. Cardoso. A large annotated medical image dataset for the development and evaluation of segmentation algorithms. [Online], Available: http://arxiv.org/abs/1902.09063, 2019.

[167] A. E. Kavur, N. S. Gezer, M. Barış, S. Aslan, P. H. Conze, V. Groza, D. D. Pham, S. Chatterjee, P. Ernst, S. Özkan, B. Baydar, D. Lachinov, S. Han, J. Pauli, F. Isensee, M. Perkonigg, R. Sathish, R. Rajan, D. Sheet, G. Dovletov, O. Speck, A. Nürnberger, K. H. Maier-Hein, G. B. Akar, G. Ünal, O. Dicle, M. A. Selver. CHAOS Challenge - Combined (CT-MR) healthy abdominal organ segmentation. *Medical Image Analysis*, vol. 69, Article number 101950, 2020.

[168] A. B. Spanier, L. Joskowicz. Automatic atlas-free multi-organ segmentation of contrast-enhanced CT scans. *Cloud-Based Benchmarking of Medical Image Analysis*, Springer, Cham, Germany, pp. 145–164, 2017. DOI: 10.1007/978-3-319-49644-3_9.

[169] F. Prior, K. Smith, A. Sharma, J. Kirby, L. Tarbox, K. Clark, W. Bennett, T. Nolan, J. Freymann. The public cancer radiology imaging collections of the Cancer Imaging Archive. *Scientific Data*, vol. 4, no. 1, Article number 170124, 2014.

[170] N. Tajbakhsh, L. Jeyaseelan, Q. Li, J. N. Chiang, Z. H. Wu, X. W. Ding. Embracing imperfect datasets: A review of deep learning solutions for medical image segmentation. *Medical Image Analysis*, vol. 63, Article number 101693, 2020. DOI: 10.1016/j.media.2020.101693.

[171] Y. Z. Zeng, Y. Q. Zhao, P. Tang, M. Liao, Y. X. Liang, S. H. Liao, B. J. Zou. Liver vessel segmentation and identification based on oriented flux symmetry and graph cuts. *Computer Methods and Programs in Biomedicine*, vol. 150, pp. 31–39, 2017. DOI: 10.1016/j.cmpb.2017.07.002.

[172] V. Verma, R. K. Aggarwal. A comparative analysis of similarity measures akin to the Jaccard index in collaborative recommendations: Empirical and theoretical perspective. *Social Network Analysis and Mining*, vol. 10, no. 1, Article number 43, 2020. DOI: 10.1007/s13278-020-00660-9.

[173] I. Rizwan I Haque, J. Neubert. Deep learning approaches to biomedical image segmentation. *Informatics in Medicine Unlocked*, vol. 18, Article number 100297, 2020. DOI: 10.1016/j.imu.2020.100297.

[174] D. Dreizin, T. N. Chen, Y. Y. Liang, Y. Y. Zhou, F. Paes, Y. Wang, A. L. Yuille, P. Roth, K. Champ, G. Li, A. McLenithan, J. J. Morrison. Added value of deep learning-based liver parenchymal CT volumetry for predicting major arterial injury after blunt hepatic trauma: A decision tree analysis. *Abdominal Radiology*, vol. 46, no. 6, pp. 2556–2566, 2021. DOI: 10.1007/s00261-020-02892-x.

[175] T. L. Fan, G. L. Wang, X. Wang, Y. Li, H. R. Wang. MSN-Net: A multi-scale context nested U-Net for liver segmentation. *Signal, Image and Video Processing*, vol. 15, no. 6, pp. 1089–1097, 2021. DOI: 10.1007/s11760-020-01835-9.

[176] J. Z. Cai, L. Lu, Z. Z. Zhang, F. Y. Xing, L. Yang, Q. Yin. Pancreas segmentation in MRI using graph-based decision fusion on convolutional neural networks. In *Proceedings of the 19th International Conference on Medical Image Computing and Computer-Assisted Intervention*, Springer, Athens, Greece, pp. 442–450, 2016. DOI: 10.1007/978-3-319-46723-8_51.

[177] Y. Zhang, B. X. Jiang, J. Wu, D. C. Ji, Y. L. Liu, Y. F. Chen, E. X. Wu, X. Y. Tang. Deep learning initialized and gradient enhanced level-set based segmentation for liver tumor from CT images. *IEEE Access*, vol. 8, pp. 76056–76068, 2020. DOI: 10.1109/ACCESS.2020.2988647.

[178] H. Y. Li, Z. X. Sun, Y. J. Wu, Y. C. Song. Semi-supervised point cloud segmentation using self-training with label confidence prediction. *Neurocomputing*, vol. 437, pp. 227–237, 2021. DOI: 10.1016/j.neucom.2021.01.091.

[179] T. M. Geethanjali, Minavathi. Review on recent methods for segmentation of liver using computed tomography and magnetic resonance imaging modalities. In *Emerging Research in Electronics, Computer Science and Technology*, Springer, Singapore, pp. 631–647, 2019. DOI: 10.1007/978-981-13-5802-9_56.

Isaac Baffour Senkyire received the B. Sc. degree in computer science from Department of Computer Science, Kwame Nkrumah University of Science and Technology (KNUST), Ghana in 2009, and the M. Sc. degree in information security and audit from Department of Computing and Information Systems, University of Greenwich, UK in 2014. He is a lecturer at Computer Science Department of Ghana Communication Technology University, Ghana. He is currently a Ph. D. degree candidate with School of Computer Science and Communication Engineering, Jiangsu University, China.

His research interests include medical image processing and pattern recognition.

E-mail: isenkyire@gctu.edu.gh

ORCID iD: 0000-0003-0160-9689

Zhe Liu received the Ph. D. degree in computer science from Jiangsu University, China in 2012. She is a visiting scholar of Department of Radiology, University of Pittsburgh Medical Center, USA, and also a professor at School of Computer Science and Communication Engineering, Jiangsu University, China. She is a member of CCF.

Her research interests include image processing, data mining and pattern recognition.

E-mail: 1000004088@ujs.edu.cn (Corresponding author)

ORCID iD: 0000-0002-1197-0390